A Numerical Study of the Impact of an Intense Squall System on Surface Cyclogenesis

by

Richard Harvey

A thesis submitted to the Faculty of Graduate Studies & Research in partial fulfillment of the requirements for the degree of

Master of Science

Department of Atmospheric and Oceanic Sciences

McGill University

Montréal, Québec

CANADA

 November, 1993

Name Richard Harvey

Dissertation Abstracts International is arranged by broad, general subject categories Please select the one subject which most nearly describes the content of your dissertation Enter the corresponding four-digit code in the spaces provided

Atmospheric Sciences — SUBJECT TERM

0 1 0 8 — SUBJECT CODE

U·M·I

Subject Categories

THE HUMANITIES AND SOCIAL SCIENCES

COMMUNICATIONS AND THE ARTS

Architecture	0729
Art History	0377
Cinema	0900
Dance	0378
Fine Arts	0357
Information Science	0723
Journalism	0391
Library Science	0399
Mass Communications	0708
Music	0413
Speech Communication	0459
Theater	0465

EDUCATION

General	0515
Administration	0514
Adult and Continuing	0516
Agricultural	0517
Art	0273
Bilingual and Multicultural	0282
Business	0688
Community College	0275
Curriculum and Instruction	0727
Early Childhood	0518
Elementary	0524
Finance	0277
Guidance and Counseling	0519
Health	0680
Higher	0745
History of	0520
Home Economics	0278
Industrial	0521
Language and Literature	0279
Mathematics	0280
Music	0522
Philosophy of	0998
Physical	0523
Psychology	0525
Reading	0535
Religious	0527
Sciences	0714
Secondary	0533
Social Sciences	0534
Sociology of	0340
Special	0529
Teacher Training	0530
Technology	0710
Tests and Measurements	0288
Vocational	0747

LANGUAGE, LITERATURE AND LINGUISTICS

Language	
General	0679
Ancient	0289
Linguistics	0290
Modern	0291
Literature	
General	0401
Classical	0294
Comparative	0295
Medieval	0297
Modern	0298
African	0316
American	0591
Asian	0305
Canadian (English)	0352
Canadian (French)	0355
English	0593
Germanic	0311
Latin American	0312
Middle Eastern	0315
Romance	0313
Slavic and East European	0314

PHILOSOPHY, RELIGION AND THEOLOGY

Philosophy	0422
Religion	
General	0318
Biblical Studies	0321
Clergy	0319
History of	0320
Philosophy of	0322
Theology	0469

SOCIAL SCIENCES

American Studies	0323
Anthropology	
Archaeology	0324
Cultural	0326
Physical	0327
Business Administration	
General	0310
Accounting	0272
Banking	0770
Management	0454
Marketing	0338
Canadian Studies	0385
Economics	
General	0501
Agricultural	0503
Commerce Business	0505
Finance	0508
History	0509
Labor	0510
Theory	0511
Folklore	0358
Geography	0366
Gerontology	0351
History	
General	0578
Ancient	0579
Medieval	0581
Modern	0582
Black	0328
African	0331
Asia, Australia and Oceania	0332
Canadian	0334
European	0335
Latin American	0336
Middle Eastern	0333
United States	0337
History of Science	0585
Law	0398
Political Science	
General	0615
International Law and Relations	0616
Public Administration	0617
Recreation	0814
Social Work	0452
Sociology	
General	0626
Criminology and Penology	0627
Demography	0938
Ethnic and Racial Studies	0631
Individual and Family Studies	0628
Industrial and Labor Relations	0629
Public and Social Welfare	0630
Social Structure and Development	0700
Theory and Methods	0344
Transportation	0709
Urban and Regional Planning	0999
Women's Studies	0453

THE SCIENCES AND ENGINEERING

BIOLOGICAL SCIENCES

Agriculture	
General	0473
Agronomy	0285
Animal Culture and Nutrition	0475
Animal Pathology	0476
Food Science and Technology	0359
Forestry and Wildlife	0478
Plant Culture	0479
Plant Pathology	0480
Plant Physiology	0817
Range Management	0777
Wood Technology	0746
Biology	
General	0306
Anatomy	0287
Biostatistics	0308
Botany	0309
Cell	0379
Ecology	0329
Entomology	0353
Genetics	0369
Limnology	0793
Microbiology	0410
Molecular	0307
Neuroscience	0317
Oceanography	0416
Physiology	0433
Radiation	0821
Veterinary Science	0778
Zoology	0472
Biophysics	
General	0786
Medical	0760

EARTH SCIENCES

Biogeochemistry	0425
Geochemistry	0996
Geodesy	0370
Geology	0372
Geophysics	0373
Hydrology	0388
Mineralogy	0411
Paleobotany	0345
Paleoecology	0426
Paleontology	0418
Paleozoology	0985
Palynology	0427
Physical Geography	0368
Physical Oceanography	0415

HEALTH AND ENVIRONMENTAL SCIENCES

Environmental Sciences	0768
Health Sciences	
General	0566
Audiology	0300
Chemotherapy	0992
Dentistry	0567
Education	0350
Hospital Management	0769
Human Development	0758
Immunology	0982
Medicine and Surgery	0564
Mental Health	0347
Nursing	0569
Nutrition	0570
Obstetrics and Gynecology	0380
Occupational Health and Therapy	0354
Ophthalmology	0381
Pathology	0571
Pharmacology	0419
Pharmacy	0572
Physical Therapy	0382
Public Health	0573
Radiology	0574
Recreation	0575
Speech Pathology	0460
Toxicology	0383
Home Economics	0386

PHYSICAL SCIENCES

Pure Sciences

Chemistry	
General	0485
Agricultural	0749
Analytical	0486
Biochemistry	0487
Inorganic	0488
Nuclear	0738
Organic	0490
Pharmaceutical	0491
Physical	0494
Polymer	0495
Radiation	0754
Mathematics	0405
Physics	
General	0605
Acoustics	0986
Astronomy and Astrophysics	0606
Atmospheric Science	0608
Atomic	0748
Electronics and Electricity	0607
Elementary Particles and High Energy	0798
Fluid and Plasma	0759
Molecular	0609
Nuclear	0610
Optics	0752
Radiation	0756
Solid State	0611
Statistics	0463

Applied Sciences

Applied Mechanics	0346
Computer Science	0984
Engineering	
General	0537
Aerospace	0538
Agricultural	0539
Automotive	0540
Biomedical	0541
Chemical	0542
Civil	0543
Electronics and Electrical	0544
Heat and Thermodynamics	0348
Hydraulic	0545
Industrial	0546
Marine	0547
Materials Science	0794
Mechanical	0548
Metallurgy	0743
Mining	0551
Nuclear	0552
Packaging	0549
Petroleum	0765
Sanitary and Municipal	0554
System Science	0790
Geotechnology	0428
Operations Research	0796
Plastics Technology	0795
Textile Technology	0994

PSYCHOLOGY

General	0621
Behavioral	0384
Clinical	0622
Developmental	0620
Experimental	0623
Industrial	0624
Personality	0625
Physiological	0989
Psychobiology	0349
Psychometrics	0632
Social	0451

This is the shortened version of the thesis:

Numerical investigation of a convectively-aided surface cyclogenesis

À ma mère et mon père, parce qu'ils m'ont permis de rêver.

RÉSUMÉ

Les dernières décennies ont vu des progrès considérables quant à la recherche sur les cyclones à développement explosif de la saison hivernale. Cependant, on a accordé peu d'attention au rôle que peuvent jouer les systèmes convectifs à la méso-échelle (SCM) sur l'évolution des cyclones extratropicaux évoluant à l'intérieur d'un environnement à faible baroclinicité. Dans cette thèse, on étudie l'impact d'un SCM sur une cyclogénèse subséquente de surface, en utilisant une simulation numérique à haute résolution, intégrée sur 36 heures, de la fameuse ligne de grain du 10-12 Juin 1985, observée lors du programme PRE-STORM. Le modèle utilisé reproduit remarquablement bien la formation initiale de la ligne de grain, puis la présence de nombreuses perturbations barométriques et circulations méso-échelle à la surface et dans les niveaux moyens, ainsi que la cyclogénèse subséquente après la dissipation du système convectif

On trouve que la ligne de grain est initiée à l'avant d'un faible front de surface avec l'aide du forçage barocline. Par la suite, l'évolution du système convectif est plus ou moins dictée par l'interaction entre les circulations internes propres au SCM et l'environnement potentiellement instable à l'avant du système. Dans cette optique, la baroclinicité environnante ne fait que pourvoir à la maintenance de conditions favorables pour l'évolution subséquente de la convection. Par ailleurs, alors que le système s'intensifie rapidement et accélère vers l'est, il modifie en même temps l'environnement barocline de grande échelle en augmentant le déphasage entre les creux thermique et barométrique de la basse et moyenne troposphère, produisant ainsi un environnement plus favorable à une cyclogénèse de surface.

Afin d'isoler le rôle de la convection humide sur la cyclogénèse de surface, deux expériences, l'une dite "humide" et l'autre dite "sèche", sont comparées. On trouve qu'en dépit de l'absence de la convection humide, le modèle arrive à produire une cyclogénèse de surface, mais avec beaucoup moins d'intensité, d'étendue verticale, et de

vitesse de déplacement. On montre que les effets de la convection humide sont non seulement d'augmenter et de diminuer, respectivement, les hauteurs des surfaces isobariques des hauts et bas niveaux, mais également de conditionner l'environnement barocline en augmentant l'angle de phase entre les ondes thermique et barométrique, ainsi qu'en intensifiant la baroclinicité de grande échelle.

ABSTRACT

Considerable progress has been made in the past decades on the life cycle of rapidly deepening winter cyclones. However, little attention has been paid to the roles of mesoscale convective systems (MCSs) in extratropical cyclogenesis that occurs within weak baroclinic environments. In this thesis, the impact of an MCS on the subsequent surface cyclogenesis is investigated, using a 36-h three-dimensional, high-resolution simulations of the famous 10-12 June squall line that occurred during PRE-STORM. The model simulates remarkably well the initiation of the squall line, numerous mesoscale surface pressure perturbations and midlevel circulation structures during the mature stage, and the subsequent surface cyclogenesis after the dissipation of the system.

It is found that the squall line is initiated ahead of a weak surface front with the aid of baroclinic forcing. Once initiated, the squall system is more of less driven by the interaction of convectively generated circulations with the potential unstable environment ahead. The baroclinic forcing only provides a favorable environment for the evolution of the squall system. As the squall system rapidly intensifies and accelerates eastward, it enhances the larger-scale baroclinicity and produces a phase-lag between the pressure and thermal waves so that the baroclinic environment is more favorable for surface cyclogenesis.

To isolate the roles of moist convection in the surface cyclogenesis, a "moist" and a "dry" simulation are compared. It is found that in the absence of moist convection the model could also produce a surface cyclone, but with much weaker intensity, much smaller extent and slower displacement. The effects of moist convection are shown not only to increase the upper-level and decrease the lower-level height of isobaric surfaces, but also to condition the baroclinic environment by increasing the phase lag between the pressure and thermal waves and enhancing the large-scale baroclinicity.

Table of contents

List of Figures

List of Tables

Acknowledgments

First and foremost, I sincerely thank my supervisor, Prof. Da-Lin Zhang, for his uninterrupted devotion and patience during the course of this research. I benefited greatly from his keen physical insights and constructive criticisms, and his mastery of mesoscale and large-scale modeling and dynamics. I gratefully acknowledge the support of Dr. Robert Benoît and Mr. Michel Valin for their kind advice during the preliminary tests at the Recherche en Prévision Numérique (RPN) of the Atmospheric Environment Service of Canada (AES). I especially thank Mr. Stéphane Bélair for his patience and generosity during the many months spent at RPN while I learned the technical aspects of numerical modeling. I also acknowledge the financial support of AES during the entire period of this master's program, and thank them for providing me with this opportunity for advancing my knowledge in meteorology. I also thank Ms. Ursula Seidenfuβ for her expert work in the preparation of the figures. The computations for this research were performed on a CRAY-YMP of National Center for Atmospheric Research, which is sponsored by the National Science Foundation.

I am indebted to my friends in the department for moral support during the long and difficult months spent in writing this thesis. I thank my office companions, Zonghui Huo and Bau Ning, for their stimulating discussions and amiable presence. Special thanks go to Thierry Reynaud for making me laugh so many times and for his constant encouragements, and to François Turcotte for sharing with me his passion for flying.

I also want to thank my long-time friend, Pierre Lang, for those fascinating discussions in which problems of the world seemed almost solvable, and for teaching me about the wonders of the Latin world.

Finally, I want to thank my family for their constant moral support and understanding throughout some difficult moments during the past two years.

Chapter 1 — Introduction

1. 1 The QPF problem

Numerical predictions of large-scale pressure systems have improved markedly during the past four decades, a fact which is largely due to the rapid increase in supercomputing power. This trend is likely to persist since it seems that this power will keep on increasing in the foreseeable future. However, such progress in large-scale prediction does not necessarily translate into the improvement of quantitative precipitation forecasts (QPFs) and severe weather warnings. This is because most of the precipitation variability occurs on scales of the order of 100 to near 1000 km, i.e., on the meso-β to meso-α scales, particularly during the warm season. Specifically, Fritsch et al (1986) found that mesoscale convective systems (MCSs) account for a large fraction of the total warm-season rainfall over the central and eastern portions of the United States. They noted that long-lived MCSs could even produce rainfall exceeding the total precipitation amounts of a hurricane. Later, Heideman and Fritsch (1988) showed that about half of the warm-season rainfall over the central and eastern U.S. was predominantly caused by mesoscale forcing mechanisms.

Therefore, in view of the current limited potential for observational networks to resolve anything less than a few hundred kilometers in length scale, and also from the fact that operational models still have coarse resolutions and often simplistic subgrid-scale parameterizations to handle mesoscale phenomena, one could speculate that the skill and accuracy of precipitation forecasts, particularly QPFs, would lower substantially during the summer months. Indeed, this presumption has been extensively verified in the literature. For example, Charba and Klein (1980) found from a study of QPFs over the United States between 1961 and 1978 that for precipitation forecasts of > 6.4 mm and

> 12.7 mm, threat scores were 33% to 55% higher during the wintertime than those during the summer. These cool-season QPF scores increased at almost twice the rate over those of the warm-season during the same period. The latter result shows an increasing gap in the quality of cool-season vs. warm-season QPFs. Similar conclusions were drawn from studies by Ramage (1982), Glahn (1985) and Sanders (1986).

Fritsch and Heideman (1989) also found very limited skill with the U.S. operational limited-area fine-mesh model (LFM) for the 1982-1983 warm-seasons. This substantiated the conclusion from Heideman and Fritsch (1988) which stated that improved QPF scores will come not only from increased model resolutions, but also from improved model physics. Also, Georgakakos and Hudlow (1984), emphasized the need for more accurate QPF information to serve as input for hydrological forecasts.

This increased concern with improved QPFs and severe weather warnings has justified a large research effort during the past few years in an attempt to improve our physical understanding of mid-latitude MCSs. Many observational studies of MCSs have uncovered a recurring array of features that they share (Newton 1950; Ogura and Liou 1980; Smull and Houze 1985, 1987; Leary and Rappaport 1987; Johnson and Hamilton 1988; Rutledge et al. 1988; Houze et al. 1989). These include: (1) a line of intense convection in which deep ascent prevails; this is followed (and sometimes preceded) by (2) an extensive area of stratiform cloud and precipitation; (3) upper-level ascent of high-θ_e air along a sloping rearward flow from the leading edge of the gust front (front-to-rear flow); (4) a descending rear inflow of mid-level low-θ_e air entering from the rear of the stratiform region (rear-to-front flow); (5) upshear tilt of convective-scale updrafts and (6) one or several mid-level mesovortices in the stratiform precipitation region (Zhang and Fritsch 1986, 1988b; Menard and Fritsch 1989; Brandes 1990; Bartels and Maddox 1991; Biggerstaff and Houze 1991b; Zhang 1992). Fig 1.1a presents a schematic cross-section of a mature squall line, showing its main convective-scale and mesoscale structure; the reader is referred to the above papers for further details.

However, the level of organization of any MCS spans a more or less continuous spectrum and ranges from the highly organized conceptual model in Fig. 1.1a, to chaotic structures where convective and stratiform precipitation are arranged randomly (Houze et al. 1990). Moreover, in studies such as Fujita (1955), Hoxit et al. (1976) and Johnson and Hamilton (1988), pressure disturbances due to squall lines were investigated in detail, using dense observations. They identified three primary features in the surface pressure patterns of MCSs that are trailed by stratiform regions: pre-squall mesolows, squall mesohighs, and wake-lows (cf. Fig. 1.1b). In particular, Johnson and Hamilton (1988) showed that wake-lows are the result of subsidence warming in the rear-to-front inflow, which was sufficiently strong just behind the stratiform precipitation region to offset evaporative cooling.

A number of numerical studies of MCSs have also been undertaken in the recent years. In particular, numerical studies such as Zhang and Fritsch (1986, 1987, 1988a), Zhang (1989), Zhang et al. (1989) and Zhang and Gao (1989) have demonstrated the potential feasibility of simulating the internal structure of MCSs using conventional observations as initial conditions. In fact, these investigations showed the importance of combining compatible model resolution with suitable model physics in order to explicitly simulate the internal structure of MCSs. This gives hope to future improvements of operational QPFs, in addition to increasing our understanding of the physical mechanisms prevalent in MCSs. These numerical studies have provided high resolution, dynamically consistent data to help understand the physical processes of features, such as the rear inflow (Zhang and Gao 1989; Zhang 1992, surface pressure perturbations, mesovortices a id stratiform precipitation (Zhang and Gao 1989), that had already been documented by Johnson and Hamilton (1988), Rutledge et al. (1988) and Augustine and Zipser (1987).

a)

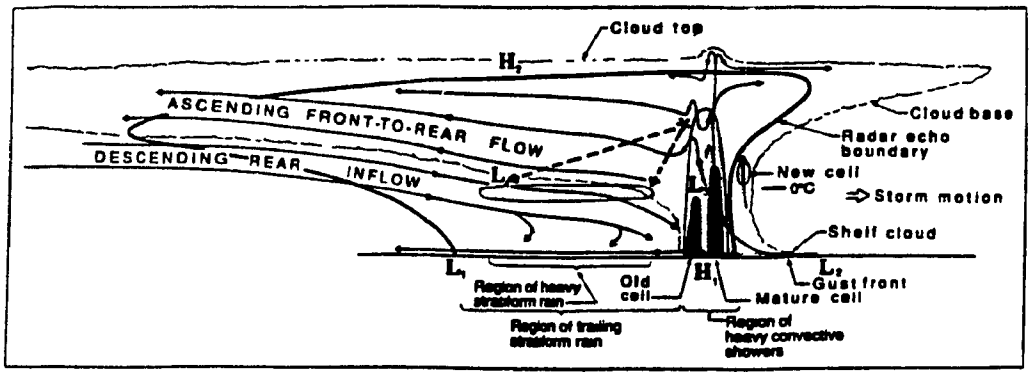

b)

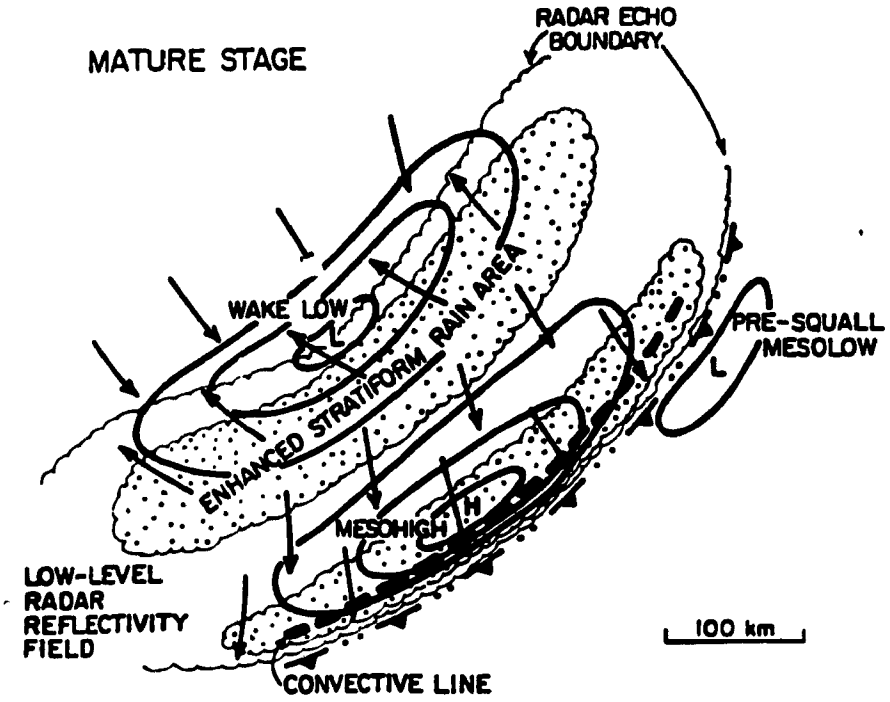

Fig. 1.1 (a) Schematic cross section of a squall line with a trailing stratiform region, oriented perpendicular to the system, and parallel to its motion; taken from Houze et al. (1989). (b) Schematic surface pressure, wind fields and precipitation distribution during the squall line mature stage; taken from Johnson and Hamilton (1988). Arrows indicate *relative* flow in (a), and *actual* flow in (b). Note that horizontal scales differ in the two schematics.

1.2 The effects of MCSs on the large-scale environment

Numerous observations have recently shown that during the growing season MCSs often form to the lee of the Rocky Mountains and undergo multiple life cycles before reaching the Atlantic Ocean (Wetzel et al. 1983; Bosart and Sanders 1981; Murphy and Fritsch 1989). Some of these systems, which are strong and well organized, could produce important influences on large-scale flow, particularly when interacting with baroclinic systems of weak to moderate intensity. Although these systems account for a substantial fraction of warm-season rainfall, little effort has been made to study the interaction of deep convection with baroclinic systems owing to limited high-resolution observations. In this thesis, we will examine the processes taking place in surface cyclogenesis after the dissipation of an MCS and provide evidence to support the hypothesis that *organized MCSs could produce a significant impact on large-scale circulations.* This hypothesis is also plausible when considering that lower static stabilities in the summer tend to decrease the average wavelength of baroclinic waves as compared to the winter (Staley and Gall 1977), making some systems comparable in size to MCSs. We hope in this way to improve understanding of the large-scale cyclogenesis problem by extending research to summertime cases, complementing the numerous winter-time case studies of more intense and often explosive cyclogenesis, for which dynamical processes tend to dominate.

The effects of deep convection on atmospheric circulations have been studied for many years. Previous studies can be categorized into two groups: (i) effects on large-scale circulations and (ii) effects on mesoscale circulations. Maddox (1983), for instance, discussed how MCSs tend to produce a persistent temperature perturbation in the upper troposphere, causing a readjustment of the mass field on the large-scale. On the other hand, Houze (1977), Zhang and Fritsch (1987; 1988b), Brandes (1990), Bartels and Maddox (1991), Biggerstaff and Houze (1991b), Zhang (1992) and Johnson and Bartels (1992), showed that convection tends to generate mesovortices of different sizes. The

presence of convectively generated mesovortices, such as those examined by Wetzel et al. (1983) and Fritsch et al. (1993), appears to explain why some MCC's could remain coherent for several days as they traveled eastward from the foothills of the Rockies toward the Atlantic Ocean. These studies provide some observational evidence that mesoscale and large-scale events following the initial outbreak of deep convection can be significantly different from those predicted by models with inadequate resolution and/or overly simplistic model physics (Heideman and Fritsch 1988). This underlines the necessity to provide realistic model forecasts of the development and evolution of MCSs, since the atmosphere is highly nonlinear, with interactions of processes from cloud microphysics to convective drafts and large scale pressure systems,

1.3 Objectives of the thesis

The purpose of this thesis is to study surface cyclogenesis events after dissipation of an MCS, using a 36-hour numerical simulation of the famous 10-11 June 1985 squall line that occurred during the Preliminary Regional Experiment for STORM-Central (PRE-STORM, see Cunning, 1986), with the Pennsylvania State University/National Center for Atmospheric Research (PSU/NCAR) Mesoscale Model, Version 4 (MM4) (Anthes and Warner 1978; Anthes et al. 1987). The life cycle of this MCS has been extensively examined, for example, by Augustine and Zipser (1987), Johnson and Hamilton (1988), Rutledge et al. (1988), Zhang et al. (1989), Zhang and Gao (1989), Zhang and Cho (1992) and Zhang (1992). Specifically, Johnson and Hamilton (1988) mentioned that after the squall system dissipated, a significant short wave trough closely associated with the system resulted in surface cyclogenesis farther east over Ohio Valley. Yet it is unclear how this cyclogenesis occurred. In particular, is there any relationship between the development of the squall line and the subsequent surface cyclogenesis? If there is, how did the squall line assisted the surface cyclogenesis? What is the relative role of the midlevel short-wave trough, and how did it interact with the squall line?

Thus the specific objectives of this thesis pertaining to the physical understanding of the surface cyclogenesis are given as follows.

(i) Extend the previous simulation of the squall line by Zhang et al. (1989) to 36 hours, i.e., valid at 0000 UTC 12 June 1985, when the surface cyclone is well developed.

(ii) Document the sequence of events from the dissipation of the squall line to the development of the surface cyclone.

(iii) Investigate different dynamical processes taking place in the surface cyclogenesis, and particularly, examine the effect of deep convection and its interaction with the large-scale baroclinic environment.

(iv) Determine the impact of the mesoscale circulation, such as mesovortices, descending rear inflow, surface pre-squall and wake lows, on the surface cyclogenesis.

The presentation of the thesis is organized as follows. Chapter 2 summarizes the model features and initial conditions used for the simulation. Chapter 3 presents a synoptic description of the case from 1200 UTC 10 June to 0000 UTC 12 June 1985, and shows verification of the simulation against conventional, mesoscale and satellite observations. Chapter 4 compares sensitivity simulations with and without convection, and discusses the impact of the squall line and large-scale baroclinity on the surface cyclogenesis. A summary and conclusions are given in Chapter 5.

Chapter 2 — Model description

The model used for this study is an improved version of the PSU/NCAR three-dimensional (3D), hydrostatic, mesoscale model as described by Anthes and Warner (1978) and Anthes et al. (1987). It has been successfully used, among others, by Zhang et al. (1989) (hereafter ZGP) and Zhang and Gao (1989) (hereafter ZG) for 21-hour numerical simulations of the 10-11 June squall system, with an almost identical version as in the present study. The improvements made to the model in these recent studies were necessary in order to address numerical simulations of the meso-β scale structure and evolution of MCSs that occurred during the warm season (Zhang and Fritsch 1986). A summary of the MM4 model system is presented in Table 2.1. The model dynamics will be described briefly in §2.1, while certain aspects of the physics will be dealt with in more details in §2.2. The initialization of the model will be discussed in §2.3.

2.1 Model dynamics

The governing equations of the model are basically those used in the original version described by Anthes and Warner (1978). The equations predict the temporal evolution of u, v, T, q and p_S, where p_S is the surface pressure, and they are written in the terrain-following sigma (σ) vertical coordinate:

$$\sigma = \frac{p - p_t}{p_s - p_t}$$

where p is pressure and p_t is the pressure at the top of the model atmosphere (p_t = 70 hPa). The effect of virtual temperature is included in the ideal gas law. For the interested reader a complete list of the governing equations is given in Anthes et al. (1987).

The model uses a self-nesting strategy in which a fine-grid mesh (FGM) with a grid-size of 25 km is embedded in a coarse-grid mesh (CGM) with a grid-size of 75 km

(Fig. 2.1). Both meshes are "staggered" in the horizontal and vertical (Fig. 2.2). In the horizontal staggering, momentum variables are defined at "dot" points while all the other variables are defined at "cross" points, which allows for more accurate calculation of the pressure-gradient force and horizontal divergence, according to Arakawa and Lamb (1977). In the vertical staggering, the vertical velocity in σ-coordinates ($\dot{\sigma}$) is computed on full σ-levels, while all the other variables are defined on half σ-levels. The numbers of grid points for (x, y, σ) dimensions of the CGM and the FGM are 55×41×19 and 106×49×19, respectively. The 19 σ-layers used for this study are obtained from the 20 σ-levels: 1.0, 0.997, 0.957, 0.901, 0.845, 0.789, 0.733, 0.676, 0.619, 0.562, 0.501, 0.440, 0.380, 0.321, 0.263, 0.206, 0.150, 0.100, 0.050 and 0.0. Fig. 2.1 shows the grid configuration used for this study. The fine mesh was positioned such that the observed cyclogenesis over Ohio Valley could be simulated and necessary high-resolution upstream disturbances could be generated and would propagate downstream to affect the cyclogenesis.

The continuous equations are spatially discretized using second-order finite differencing, while the time integration is done using a pressure averaging method first proposed by Brown and Campana (1978). This method first computes the geopotential and surface pressure values at time step $\tau + 1$ before calculating the momentum variables at $\tau + 1$. A weighted average of geopotential and surface pressure at time steps $\tau - 1$, τ, and $\tau + 1$ is used in the pressure-gradient force terms of the momentum equations. This method allows for time steps twice as large as with the more conventional leap-frog scheme.

A self-nested grid procedure is used at the interface between the FGM and CGM, allowing feedbacks between the two meshes and also permitting the use of realistic terrain (Zhang et al. 1986). The outer CGM lateral boundary, on the other hand, is

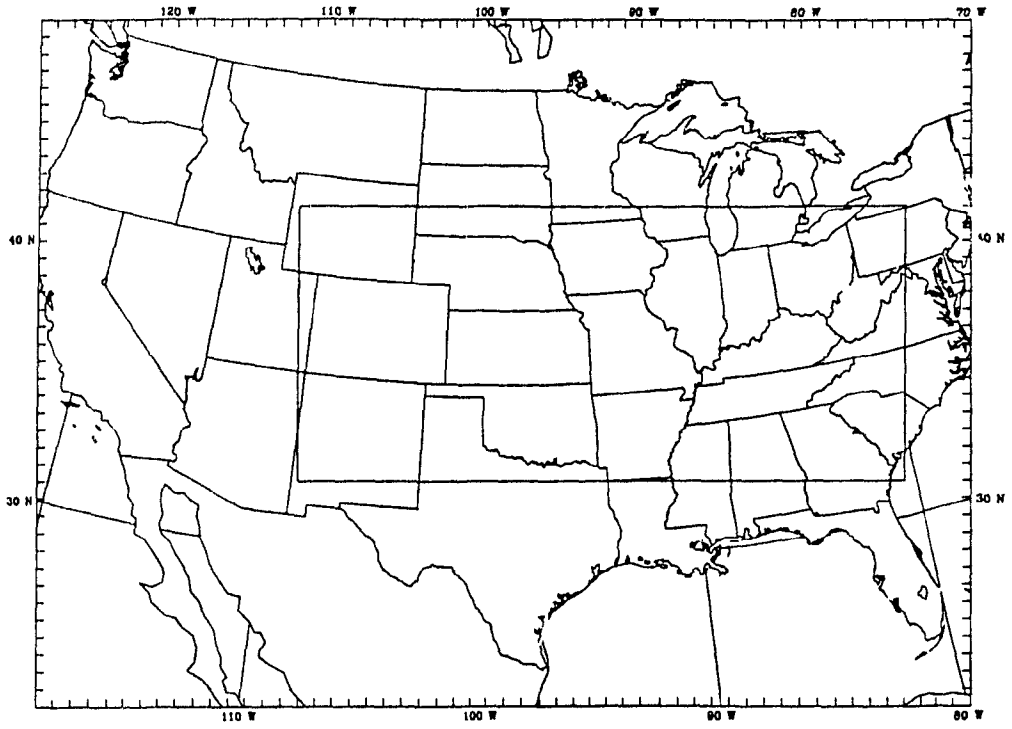

Fig. 2.1 The model nested-domain of the PSU/NCAR model used for this study. Interior box indicates the fine-mesh portion of the domain. The intervals marked on the frame are mesh grids (75 km for coarse mesh and 25 km for fine mesh).

a)

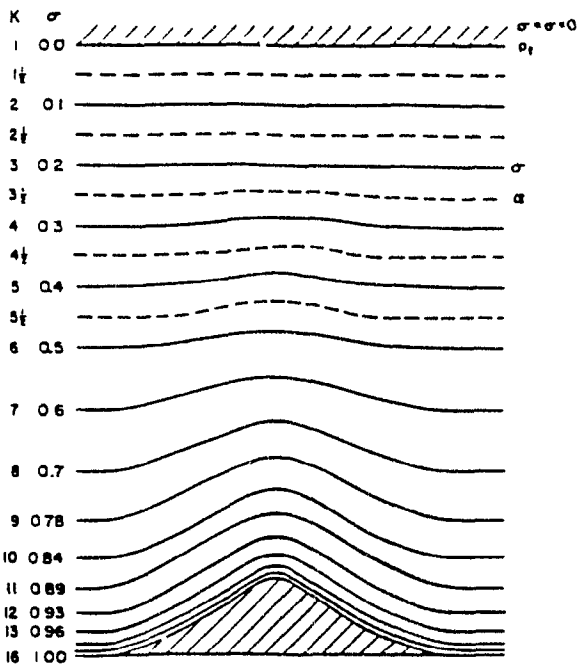

b)

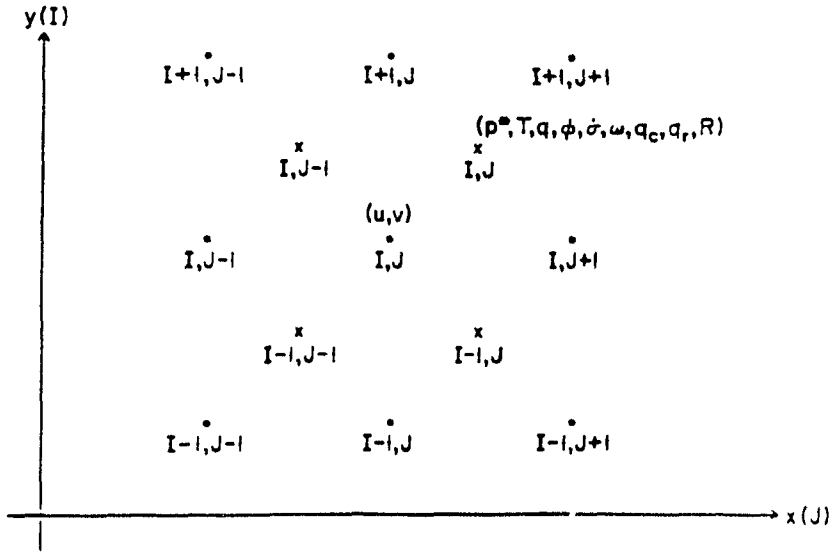

Fig. 2.2 (a) Schematic of the vertical grid structure in the PSU/NCAR model The variable $\dot{\sigma}$ is defined at the full σ-levels. (b) Schematic horizontal grid structure of the model. Both figures are taken from Anthes et al. (1987)

determined by linearly interpolating 12-hourly observations in time and specifying the resulting values according to Perkey and Kreitzberg (1976).

2.2 Model physics

a) Fritsch-Chappell and explicit schemes

It has been realized that realistic simulations of MCSs require more than simply a decrease in the horizontal grid size (Bélair et al. 1993). In particular, as the grid size decreases, solutions corresponding to more energetic convective motions become possible. On the one hand, an appropriate convective parameterization scheme is needed to include the effects of subgrid-scale updrafts, downdrafts and detrainment. On the other hand, a reasonable explicit scheme is necessary when the grid spacing is small enough to resolve meso-β scale circulations of MCSs and associated phase changes.

Thus, an improved version of the Fritsch-Chappell cumulus parameterization (Fritsch and Chappell 1980, Zhang and Fritsch 1986) is used for the fine mesh of the model, while an Anthes-H.L. Kuo (Anthes et al. 1987) convective parameterization is used for the coarse mesh. In addition, an explicit treatment of cloud water (ice) and rain water (snow) (Hsie et al. 1984; Zhang et al. 1988; Zhang 1989; Dudhia 1989) for both the CGM and FGM was utilized. These physical routines are identical to those used by Zhang et al. (1989) in their simulation of the June 10-11 squall line.

In the Fritsch and Chappell (1980) scheme, the characteristics of individual subgrid-scale convective clouds and their effects on the grid-scale variables (e.g., temperature, moisture and horizontal momentum) are parameterized by assuming that available buoyant energy (ABE), vertical wind shear and vertical motion determine the evolution of deep convection over a grid box of 20 km. It is also assumed that a single deep convective cloud dominates the vertical transport of heat and moisture, which include an updraft, a downdraft and compensating subsidence. The scheme also includes effects of parameterized freezing and melting in the column.

The explicit scheme was described in Hsie et al. (1984), Zhang (1989) and Dudhia (1989), and contains prognostic equations for cloud water (ice) and rainwater (snow). These equations take into account most of the changes between the vapor, liquid and solid phases of water, as well as effects due to hydrostatic water loading and virtual temperature. The solid and liquid phases are not allowed to co-exist, rather, an abrupt phase change takes place at the 0°C isotherm, allowing for economy of memory storage, but causing the absence of supercooled droplets in the model.

It is important to note that, as discussed in Zhang et al. (1988), the implicit and explicit schemes operate *simultaneously* in the model to account for the separate effects of subgrid-scale convective effects and grid-scale processes. Typically, condensates travel mesoscale distances before reaching the ground and hence be registered as precipitation. Therefore, mesoscale models have to explicitly predict this transport in order to realistically simulate the spatial and temporal evolution of diabatic sources and sinks due to the various phase changes of condensate before precipitating. This provides in turn a broader scale of interaction between the subgrid-scale convection and the mesoscale circulation. At the same time, an implicit convection scheme is also necessary in order to parameterize the significant subgrid-scale vertical fluxes of heat and moisture, even for a grid-size of the order of 10 km (see Zhang et al. 1988 for the discussions).

b) Planetary boundary layer and other parameterizations

The planetary boundary layer (PBL) parameterization is basically the same as that used by ZGP, Zhang and Fritsch (1986) and Zhang and Fritsch (1988b) in simulations of a number of MCSs, and is a modified version of the original Blackadar (1979) PBL model. In this scheme, the surface temperature is specified from a surface energy budget based on a "force-restore" slab model:

$$C_g \frac{\partial T_g}{\partial t} = R_n - H_m - H_s - L_v E_s + \left.\frac{\partial \theta_g}{\partial t}\right|_{CONV},$$

where C_g is the thermal capacity of the slab, R_n is the net radiation, H_m is the heat flow through the ground, H_s is the sensible heat flux into the atmosphere, L_v the latent heat of vaporization, E_s the surface moisture flux, and $\partial\theta_g/\partial t|_{CONV}$ is the ground potential temperature tendency due to deep convection taken as the tendency produced by the Fritsch-Chappell scheme for the first model layer. In the calculation of R_n, attenuation from water vapor, clouds, multiple Rayleigh backscattering and reflections from aerosols are taken into account, as well as are cloud and precipitable water influences on downward infrared radiative flux. The heat flow into the ground is computed through a simple first-order diffusion process, with the soil temperature being specified and kept fixed throughout the length of the integration. Finally, the sensible and moisture fluxes into the atmosphere are computed from similarity theory. Note that all the basic parameters required for these surface budget calculations, i.e., moisture availability, surface albedo, roughness length, thermal capacity and surface emissivity, are derived from the land-use data archived at NCAR and given by a look-up table which assigns one value of a surface index for each grid-point of the domain.

Once the surface fluxes are known, fluxes through the above stable layers are computed from *K*-theory with an implicit diffusion scheme. In the case of free convection, a PBL height is calculated, and the heat, moisture and momentum are vertically mixed following the method prescribed by Blackadar (1979) and Zhang and Anthes (1982), and later modified by Zhang and Fritsch (1986).

2.3 Model initialization and initial conditions

The model was initialized at 1200 UTC 10 June 1985 with data from conventional observations, following the method described in Zhang et al. (1986).

Briefly, the standard global National Meteorological Center (NMC) analysis was interpolated to the model coarse mesh as a first guess and then enhanced with rawinsonde observations using a successive-correction type objective analysis. Then the resulting fields were interpolated to the fine mesh and enhanced in the same manner. No balancing between the mass and wind fields was done, but the vertically integrated divergence was set to zero in order to minimize gravity wave noise in the first few hours of integration.

Figs. 2.3 and 2.4 show the model initial conditions at 700 hPa and the surface, respectively. One can see that the large-scale conditions were characterized by a relatively weak and shallow baroclinic zone to the west of the PRE-STORM network, and a mesoscale midlevel trough over eastern Wyoming and central Colorado (Fig. 2.3). Moderate cold (warm) advection prevailed behind (ahead of) the trough axis. At the surface (Fig. 2.4a), a weak cold front was located over northern Colorado with two meso-α low pressure centers, one over western Colorado at 1004 hPa and a second one over western Nebraska at 1009 hPa. The area was also dominated by large-scale cyclonic flow centered near the western Nebraska low. Moist mid-tropospheric air was accompanying the cold front and the short-wave trough above 600 hPa, with very dry air below (not shown). Ahead of this cold front, a quasi-stationary warm front extending from eastern Colorado to southern Oklahoma was associated with a southwesterly to southerly low-level flow advecting high-θ_e air into Oklahoma and Kansas (Fig. 2.4b). Overlying this moist low-level air was a much dryer air mass, suggesting the presence of considerable convective available potential energy (CAPE) along the warm front. Finally, a near-surface temperature inversion was present throughout this high CAPE

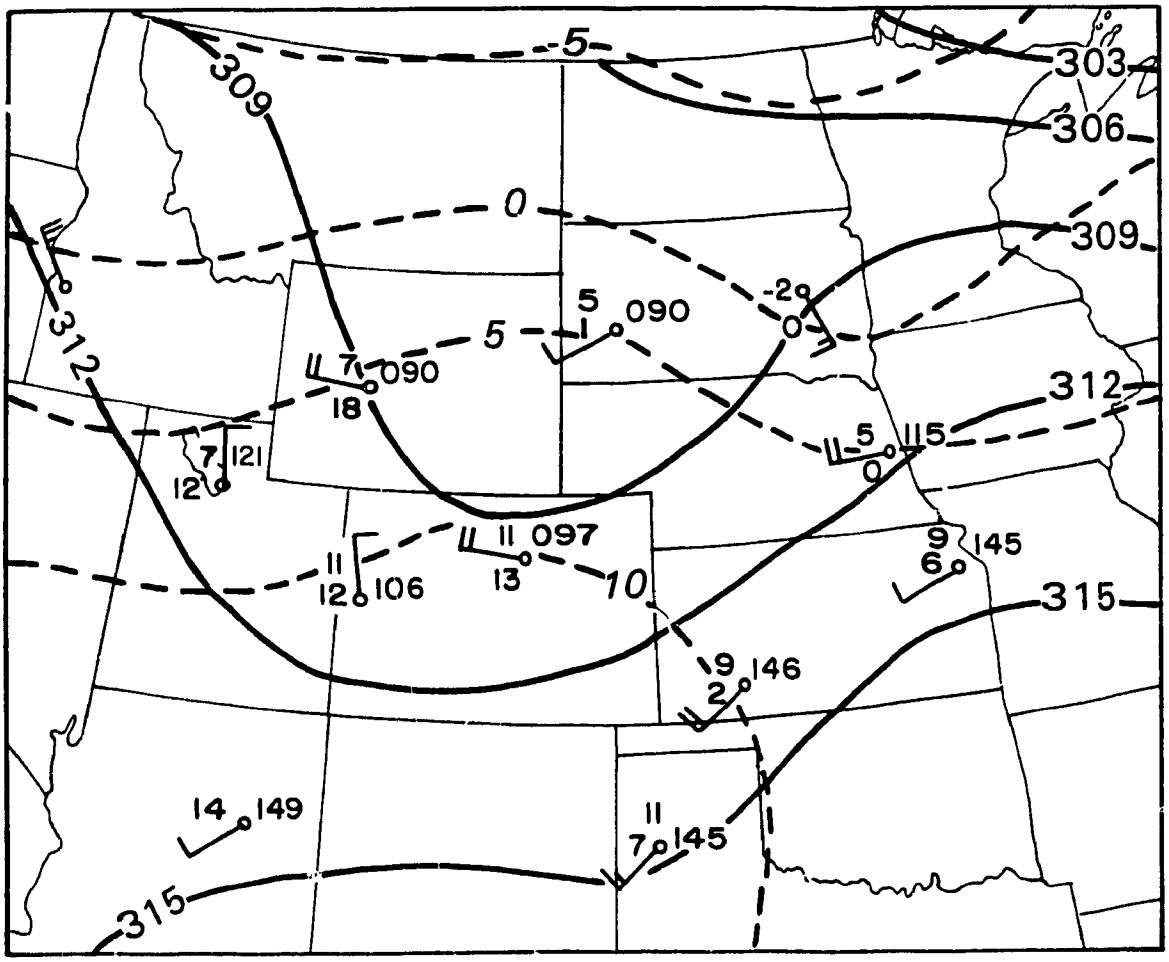

Fig. 2.3 Distribution of 700 hPa heights at intervals of 3 dam, and temperatures at intervals of 5°C for 1200 UTC 10 June 1985. A full barb is 5 ms^{-1}. Selected observations of temperature, dew-point depression, and heights are plotted using meteorological convention.

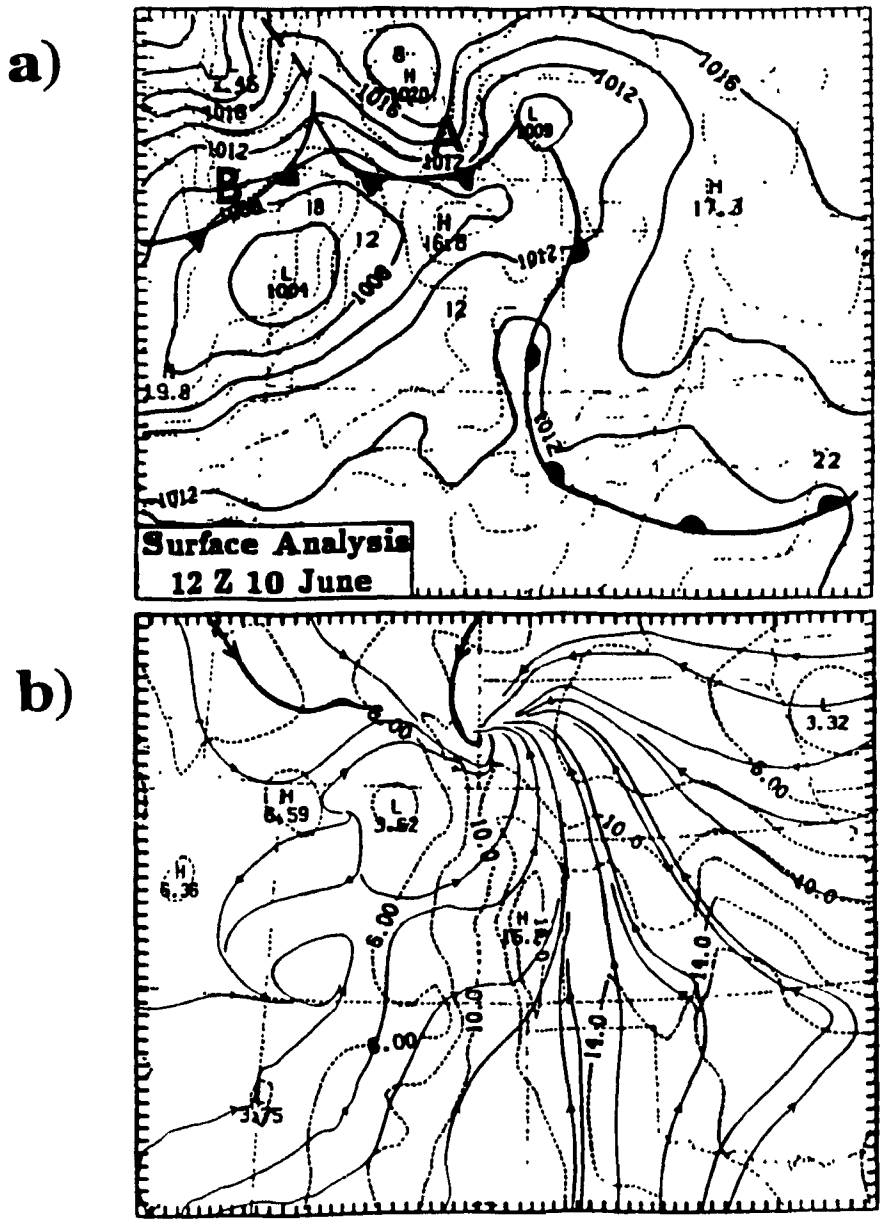

Fig. 2.4 Surface synoptic analysis for 1200 UTC 10 June 1985. (a) Sea-level pressure (solid lines), at intervals of 2 hPa, and temperature (dashed lines) at intervals of 2°C. (b) Stream lines (solid lines), and specific humidity (dashed lines) at intervals of 2 g kg $^{-1}$.

area (see ZGP), and acted momentarily as a "lid" which prevented the release of deep convective instability ahead of the cold front (Carlson and Ludlam 1968) for the first few model hours until surface heating and other environmental conditions became favorable.

TABLE 2.1 Summary of MM4

Dynamics

- Hydrostatic primitive equations, u, v, T, q and p_s predictive
- Two-way interactive nested-grid procedure (Zhang et al. 1986)
- Time-dependent outer boundary conditions for the CGM, based on regularly-spaced observations.
- Brown and Campana (1978) time discretization
- Staggered horizontal grid overlaid on a Lambert conformal map projection (25 km grid length for the FGM and 75 km for the CGM)
- 19 staggered σ-levels (normalized pressure) with top at $p_t = 70$ mb
- Time step of 40 s for FGM and 120s for the CGM
- Fourth-order horizontal diffusion

Physics

- Fritsch-Chappell (1980) convective parameterization scheme for the FGM which includes moist downdrafts, anvil evaporation, precipitation efficiency $\propto$ to vertical wind shear and cloud base height and water vapor detrainment to the grid-scale
- Anthes/Kuo type convective parameterization for the CGM (Anthes et al. 1987)
- Explicit moisture scheme with predictive equations for cloud water (ice) and rain water (snow) and bulk treatment of the microphysics (Hsie et al 1984, Zhang et al 1989)
- Modified Blackadar (1979) PBL treatment (Zhang and Anthes 1982)
- Surface fluxes computed from similarity theory
- Implicit vertical diffusion
- Prediction of ground temperature following the force-restore "slab" model

Chapter 3 — Case description and model verification

In this chapter we will document the sequence of events from the model initial time to the genesis of the surface cyclone. We will base our description on observations using NMC standard pressure-level and surface analyses, enhanced infrared satellite imagery from the Geostationary Operational Environmental Satellite (GOES), and mesoanalyses from Johnson and Hamilton (1988; hereafter referred to as JH88). The numerical simulation will also be used to provide additional details unresolved by the observations. In order to trace the evolution of the surface features as the squall system moves out of the PRE-STORM network, the surface maps were manually reanalysed by combining the original NMC data and the JH88 analyses. This will also allow us to describe more clearly the relationship between the convectively generated perturbations and their larger-scale environment. For the sake of clarity, not all the data used for the analyses were plotted. Because of the use of available special network data, mesoscale details over the network during 0300 and 0600 UTC 11 June can be analyzed with more confidence. For other times and locations, mesoscale details were inferred from the available NMC surface data and from temporal continuity.

We will first describe briefly the pre-cyclogenesis period from 1200 UTC 10 June to 0600 UTC 11 June, since a number of other studies have covered the evolution of the squall system during this period (e.g., JH88; Rutledge et al. 1988; ZGP). Then we will document in detail the remaining 18 h in order to clearly identify the events leading to the large-scale surface cyclogenesis, as has been noted by JH88. We will close the chapter by examining the effects of the squall system on the large-scale flow during the 36-h period.

3.1 Pre-cyclogenesis stage

Both JH88 and ZGP showed that the squall line was initiated at 2100 UTC 10 June ahead of the surface cold front (i.e., the segment "A" in Fig. 2.4) after it passed over the Rocky Mountains and interacted with the quasi-stationary warm front. The midlevel short wave has also contributed to the development and organization of the squall system. Then, the system intensified rapidly within a widespread convectively unstable environment over the network and propagated southeastward at a speed of 14-16 m s^{-1}. The daytime boundary-layer development and the transport of high-θ_e air in the low-level southerly current provided such a favorable condition for rapid amplification (e.g., JH88; ZGP). During the intensifying stage, both the radar echoes and satellite imagery show intense convective cells along the leading line and rapid expansion of stratiform cloudiness behind (Rutledge et al. 1988; Biggerstaff and Houze 1991a).

By 0300 UTC 11 June, the squall line has reached its peak intensity with vigorous convective-scale and mesoscale circulations. In particular, three distinct airflows as shown in Fig. 1.1a have developed: an overturning updraft along the leading line, a front-to-rear (FTR) ascending flow associated with the generation of the trailing stratiform precipitation, and a rear-to-front (RTF) descending flow (JH88; ZGP). In addition, Biggerstaff and Houze (1991b) and Zhang (1992) showed the development of a midlevel mesovortex in the trailing stratiform region of the squall system. At the surface, Fig. 3.1 exhibits the typical pressure perturbations of midlatitude squall lines, i.e., a pre-squall mesolow, a squall mesohigh and a wake low (JH88; ZGP). ZGP have traced the evolution of the pre-squall mesolow back to the mesolow ahead of the surface front over western Nebraska at the model initial time (see Fig. 2.4). Zhang and Gao (1989) and JH88 showed that the mesohigh was generated by convective downdrafts and evaporation of stratiform precipitation in the descending rear inflow, whereas the wake low developed hydrostatically as a consequence of adiabatic warming by descending rear inflow beneath the stratiform cloudiness. The intense convective downdrafts and descending rear inflow

also accounted for the rapid propagation of the squall system. Note that these pressure perturbations depart substantially from the pressure pattern at the model initial time (cf. Figs. 2.4 and 3.1), indicating the significance of convective forcing. Despite their continued intensification, these disturbances were embedded in a large-scale weak cyclonic circulation, with a surface trough, coinciding with the pre-squall mesolow, that extended northeastward to Ohio Valley. A small low pressure center of 1010 hPa could also be analysed near the western end of a stationary front running along the large-scale trough. Because of the significant convective forcing, this low and the pre-squall trough were basically overwhelmed by the squall-line circulation.

Radar and satellite observations revealed that the squall line entered a stage of rapid decay after 0300 UTC (JH88; Rutledge et al. 1988), as it advanced into a convectively less unstable environment to the east of the PRE-STORM network. At 0600 UTC 11 June the squall line was well into the dissipation stage; it was characterized by weak convective cells along the leading line and weak FTR ascending flow in the stratiform region (see ZGP). As a result, the pre-squall mesolow became less controlled by convective forcing. Instead, a closed surface low began to emerge to the northeast of the squall system where the convective forcing was likely the weakest. This roughly marks the onset of the surface cyclogenesis. By contrast, the descending rear inflow still maintained its intensity, because there were a large amount of condensate available for evaporation (see Zhang and Gao 1989). Thus, the intensity of the mesohigh and wake low were sustained even during this decaying stage. Note that the wake low has split into two segments: one over western Oklahoma and the other over eastern Kansas; they tended to move southeastward and northeastward, respectively.

We begin to verify the model simulation against the detailed observations starting with the 18-h simulation, and using a larger domain (see Fig. 3.2b) as compared to that given in ZGP. It is apparent that the model reproduces extremely well the pre-squall

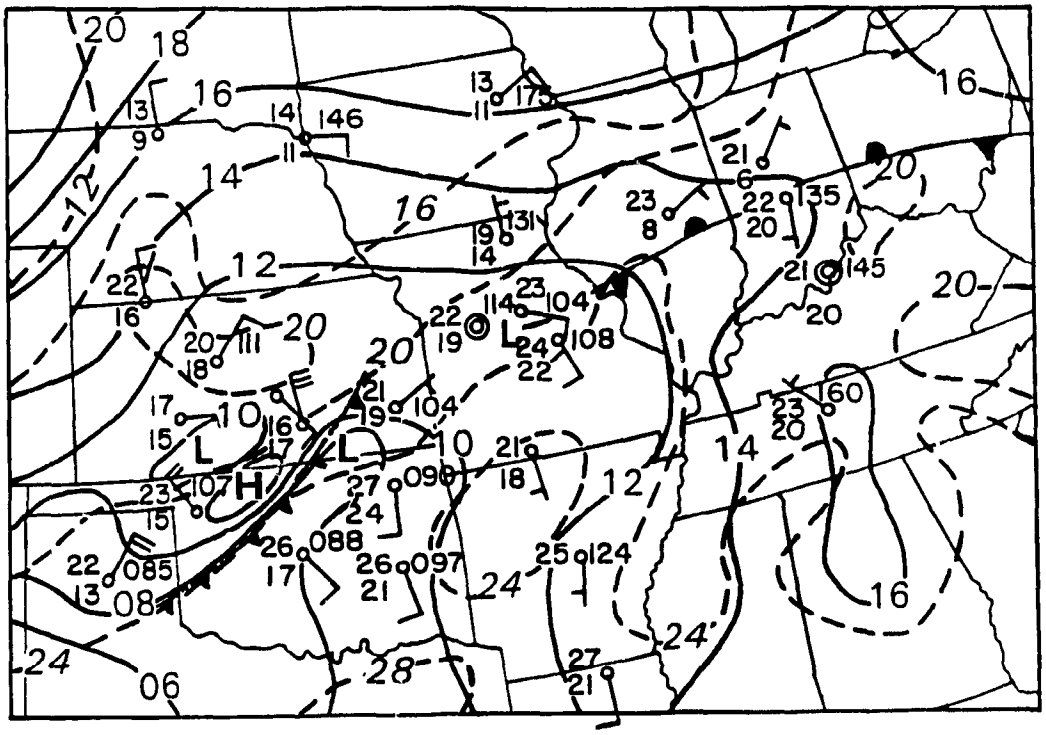

Fig. 3.1 Mesoscale analysis of sea-level pressure (solid lines) at intervals of 2 hPa, and surtace temperature (dashed lines) at intervals of 4°C for 0300 UTC 11 June 1985. Gust fronts are indicated by double-dot dashed lines with triangles. A full wind barb is 5 ms^{-1}. Cold and warm fronts, and selected observations of temperature, dew-point temperature, and pressure are plotted using meteorological convention. Pressures are labeled with the thousands and hundreds omitted; e.g., "06" = 1006 hPa.

a)

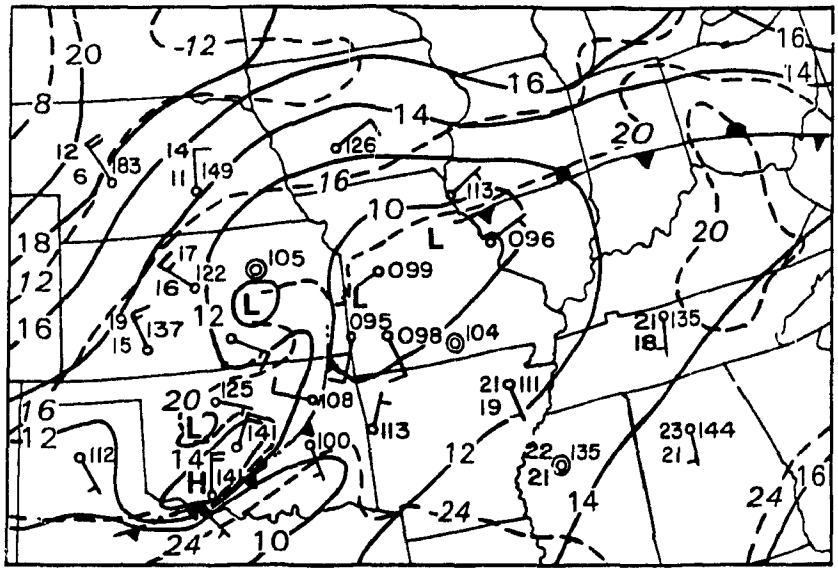

b)

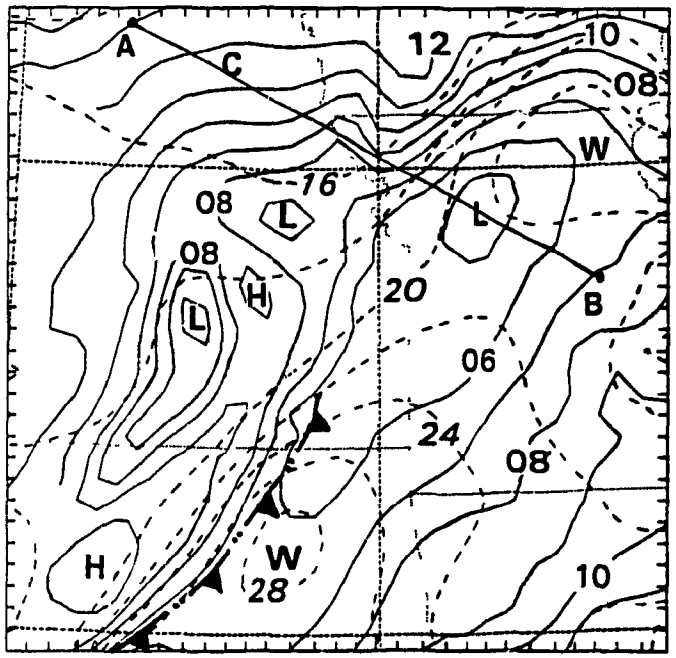

Fig. 3.2 (a) As in Fig. 3.1 but for 0600 UTC 11 June 1985. (b) Distribution of sea-level pressure (solid lines) at intervals of 1 hPa, and surface temperature (dashed lines) at intervals of 2°C for the 18 h simulation. Line A-B in this figure and Figs. 3.4b and 3.5b denotes positions of vertical cross-sections used in Fig. 4.6.

mesotrough to the east, the convectively generated mesohigh and the northern wake low over eastern Kansas (the southern wake low, although reproduced by the model, cannot be seen in Fig. 3.2b). More importantly, the model simulates well the development of the closed surface low to the northeast of the squall system, except that it is more compact compared to the observations. This discrepancy is attributable to the lack of high-resolution surface observations over Missouri. The basic pressure pattern and temperature distribution are also reasonably simulated; they are also superposed upon the large-scale surface trough system. It should be noted that the horizontal extent of this surface trough is much more extensive than that at the model initial time, and in a sensitivity run, in which the influence of the squall system was omitted (see Fig. 18 in Zhang and Gao 1989). This indicates the significant feedback effects of the squall system on its larger-scale environment.

3.2 Cyclogenesis stage

At 0900 UTC, most of the squall system has displaced out of the PRE-STORM network. Radar reflectivities at 0800 UTC exhibit the last few rapidly weakening convective cells along the leading edge, followed by tenuous echoes from the two dissipating stratiform regions (see Rutledge et al. 1988), as could also be identified from the satellite imagery (Fig. 3.7b). As a result, the convectively induced pressure perturbations were becoming much weaker and less distinct (see Fig. 3.3). For instance, the southern wake low had been absorbed by the larger-scale surface trough as it moved southeastward. The mesohigh had visibly shrunk in size and become more or less a mesoridge; it was about to disappear as the stratiform rain ceased. Meanwhile, the northern wake low was crossing the Kansas-Missouri border and it was evidently merging with the major surface low located over central Missouri. Notably, this merging process coincided with a somewhat greater organization of the background flow, as indicated by closed

isobars of 1010 and 1012 hPa. It also coincided with the deepening of the major surface low.

Very similar events also occurred in the 21-h model simulation (see Fig. 3.3b). In particular, the model simulation shows more clearly how the merging process takes place. That is, as the convective forcing rapidly weakens, the wake low advances northeastward at a rate roughly twice as large as that of the major surface low. This process seems to assist the more rapid deepening of the surface low during this period, since warmer air associated with the wake low is being displaced into the column above the major low. Its central pressure decreases from 1005 hPa at 18 h (Fig. 3.2b) to 1003 hPa at 21 h (Fig. 3.3b) and 1001 hPa at 24 h (Fig. 3 4b). It should be mentioned that the modeled central pressure is about 5 hPa deeper than the observed. This could be attributed partly to the lack of high-resolution observations, and partly to the use of different pressure reduction procedures to compute the sea-level pressure (see Zhang and Fritsch 1986 for the related discussions). Nevertheless, the simulated basic patterns are in good agreement with the observed.

By 1200 UTC 11 June, the squall line activity had entirely ceased, and chaotic cloud fragments were passively advected by the large-scale flow (cf. Fig. 3.7c and 3.8b). However, a more significant spin-up of the large-scale cyclonic circulation occurred as the mesoscale pressure disturbances finally merged into a single pressure center near the Missouri-Illinois border (see Fig. 3.4). Surface winds in the vicinity of the center, which were never more than 2-3 m s^{-1} before, increased to northeasterly at 7-8 m s^{-1} on its northern flank. This suggests the development of stronger surface convergence and subsequent generation of cyclonic vorticity through vortex stretching. Meanwhile, these strong winds advected more cold air southward to enhance a cold front along the trough axis. For example, note how the 16°C isotherm, which had remained north of Missouri, rapidly moved into the northern part of the state at 1200 UTC (cf. Figs. 3.1-4). Less apparent but still visible is weak warm advection ahead of the cyclone, as stations in eastern Arkansas and Missouri reported a 1-2°C warming over the past 3 hours. These

a)

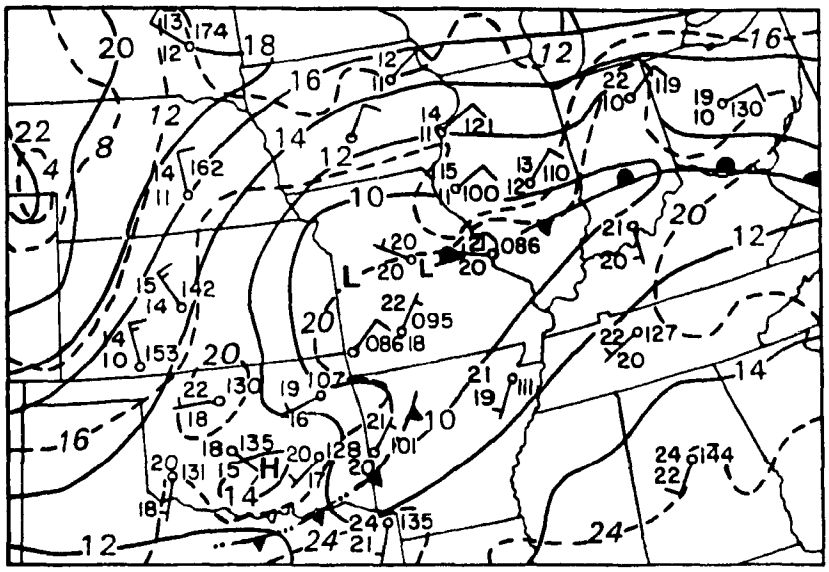

b)

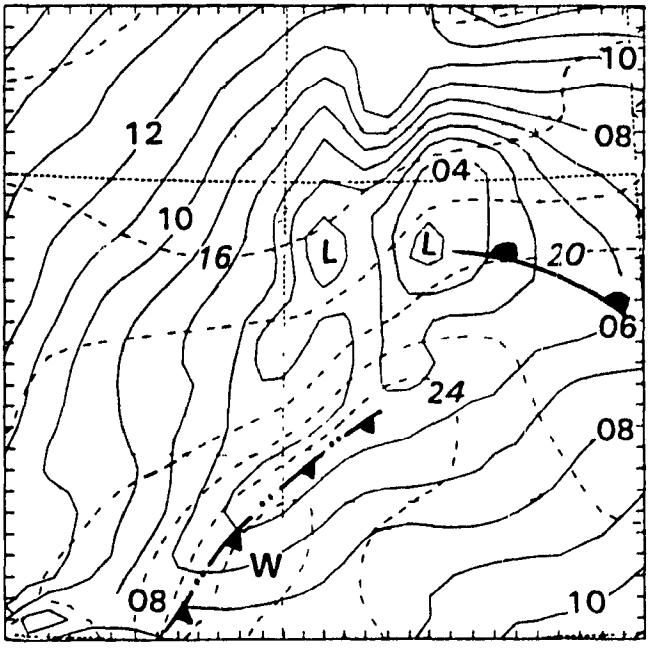

Fig. 3.3 As in Fig. 3.2 but for 0900 UTC 11 June.

a)

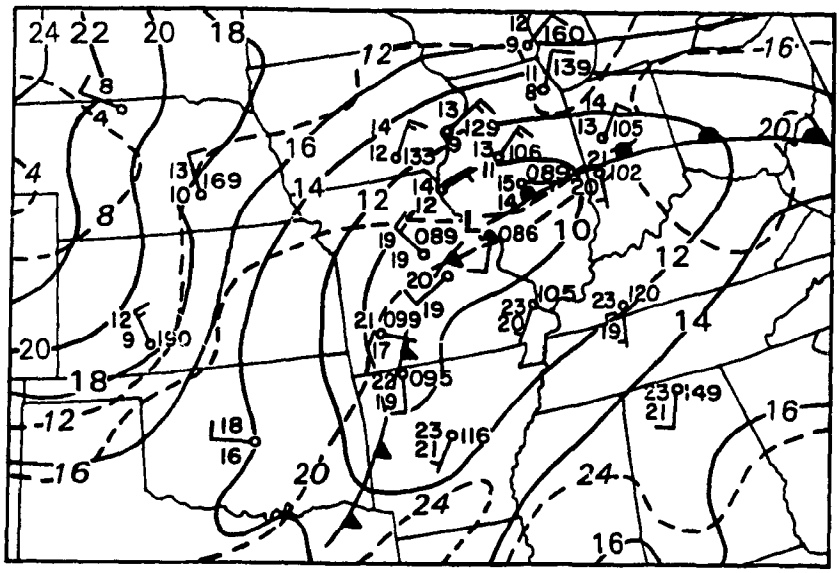

b)

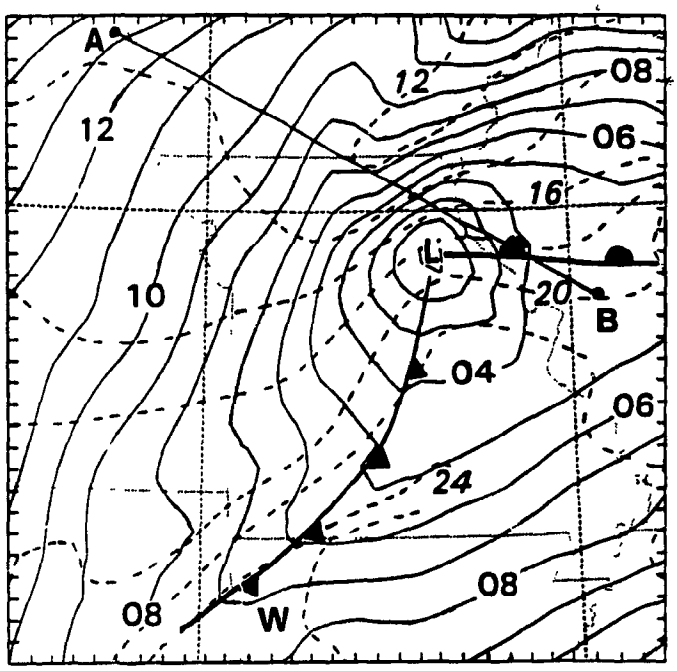

Fig. 3.4 As in Fig. 3.2 but for 1200 UTC 11 June.

simultaneous increases in the cold and warm advection are indicative of baroclinic energy conversion for surface cyclogenesis. It is remarkable that during this short time period the "background" flow has adjusted to the existing mass field and quickly become a typical developing extratropical storm, particularly when considering that the flow near the cyclone center still remained light and variable three hours earlier. This cyclonic spin-up occurred only after the *complete* demise of the squall system. Two conclusions could be tentatively drawn from these results. On the one hand, the squall system must have played a crucial role in the spin-up of the surface cyclone, since a smooth transition from the squall's pressure perturbations to the large-scale cyclone was observed over the past 6 hours. On the other hand, the large-scale baroclinity, which was obscured by the convective forcing, now came into play in the subsequent evolution of the surface cyclone. A thorough examination of these conclusions will be undertaken in the next chapter.

The model also reproduces very well the timing and the location of the final merging and subsequent surface cyclogenesis (Fig. 3.4b). The baroclinic development processes are more clearly apparent in the simulation. For example, strong cold advection occurs to the north and west of the cold front and weak warm advection occurs to the east, a pattern for a typical "synoptic wave". This baroclinic development has resulted in a packing of the isotherms just north and west of the low center, and more circular-shaped isobars near the center but still elongated structure at a larger scale. These results are very encouraging when considering that they are generated from conventional-data produced initial conditions. The results indicate that the model physical representations used for this study are realistic enough to reproduce the life cycle of the squall system and its effects on the larger-scale environment.

Another impact of the squall line on the formation of the surface cyclone is the cold frontogenesis that appeared to be greatly influenced by the squall's gust front. Specifically, both the observations and simulation show that as the gust front moved out of Oklahoma, the squall line left in its wake an extensive pool of cold air mass. This cold

pool, although no longer forced by convective downdrafts, continues to propagate southeastward with the surface trough, and thus it acts as a cold front with sharp cross-frontal wind shifts over western Arkansas.

In the absence of organized deep convection, the evolution of the surface cyclone was governed by baroclinic processes over the next 12 hours. Most notable during this stage was the rapid eastward acceleration and the intensification of the cyclone. By 1800 UTC 11 June, the cyclone had already crossed over to southwestern Indiana and had deepened by a full 3 hPa to 1005 hPa (Fig. 3.5a). Moreover, the cyclonic flow continued to intensify, with wind reports of over 10 m s^{-1} in the northwestern quadrant and 5-8 m s^{-1} in the warm sector. This led to more significant increases in temperature gradients and the genesis of the surface fronts along the baroclinic wave. Clearly, the increased cold and warm advection indicates the generation of more kinetic energy through baroclinic processes and the further amplification of the surface cyclone. Around this noon time, the satellite imagery shows an extensive shield of midlevel cloud tops to the north and northeast of the cyclone and a band of convection to the south (see Fig. 3.7d), which resembles the commonly observed comma-shaped cloud pattern of extratropical cyclones. Notice the significant heating of the boundary layer in the warm sector of the cyclone where surface temperatures had increased from 24°C to 30°C during the last 6 hours. This surface heating was likely responsible for the development of the convective band along the cold front. This convective development would clearly have some effect on the further intensification of the surface cyclone; but the effect should be relatively weak because of its much less horizontal extent compared to baroclinic forcing.

As compared to the observations, the simulated storm appears to move slightly slower (cf. Figs. 3.5a,b), and shows a lesser deepening rate with only a 1 hPa decrease in central pressure as compared to 3 hours earlier. In spite of these minor differences, the rapid acceleration of the cyclone and its related development are well reproduced. The position and intensity of the cold front, the stronger flow in the northwestern quadrant and

a)

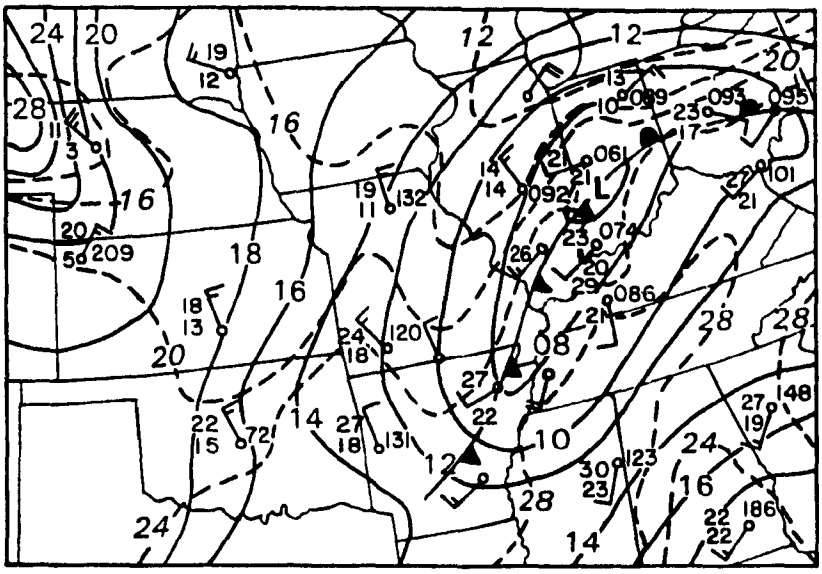

b)

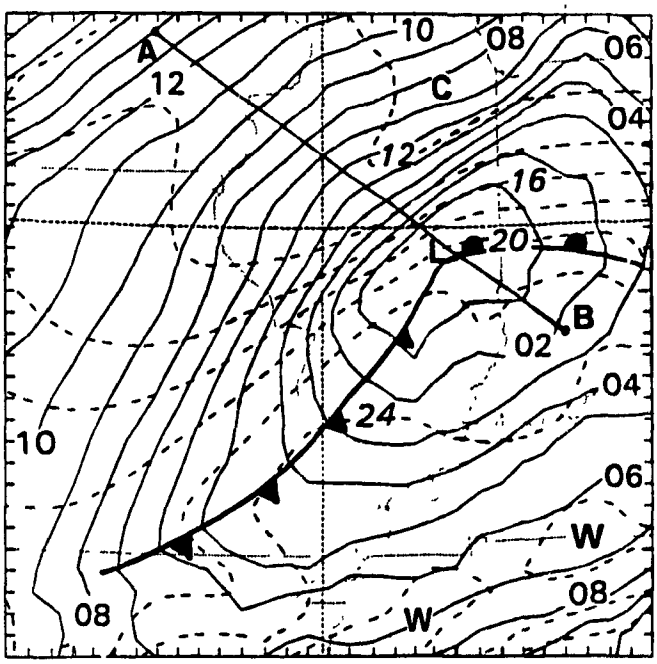

Fig. 3.5 As in Fig. 3.2 but for 1800 UTC 11 June.

the general southwest-northeast orientation of the storm were also reasonably handled. Finally, the boundary layer heating in the warm sector of the cyclone is reproduced with reasonable accuracy, as model surface temperatures increase from 24 to over 28°C.

At the end of our period of interest (i.e., 0000 UTC 12 June), both the observations and simulation show a further deepening of the cyclone, with intensified surface flow and continued stronger cold advection behind the cold front (see Fig. 3.6). In particular, a 15 m s^{-1} wind was reported over Lake Erie, about 200 km to the north of the cyclone. Observations also revealed the expansion of the convective band associated with the cold front (see Fig. 3.7e) and an intense frontal zone close to the surface cyclone. After this time the storm continued its deepening to 997 hPa as it moved into the Atlantic Ocean 18 hours later (not shown).

3.3 Evolution of the larger-scale flow

So far we have examined the evolution of the surface flow throughout the life cycle of the squall system and the subsequent cyclogenesis, and we have shown evidence to suggest that the squall line had an impact on the formation of the cyclone. Now let us inspect the evolution of the midlevel disturbances and examine whether the squall system also had an influence on the larger-scale tropospheric flow. Fig. 3.8 shows the observed 700 hPa heights and temperatures at 0000, 1200 UTC 11 June and 0000 UTC 12 June. At 0000 UTC 11 June, the squall line had been active for more than 3 h and it was now located just ahead of the 700-hPa short-wave trough axis (cf. Fig. 6d in ZGP and Fig. 3.8 herein), that was oriented from central Nebraska to the Oklahoma panhandle. Note that a thermal ridge, coinciding with the trough axis at the model initial time, had disappeared during this period (cf. Figs. 2.3 and 3.8a). Instead, a larger-scale weak thermal trough was formed behind the height trough, still providing the continued cold advection to the rear of the system.

a)

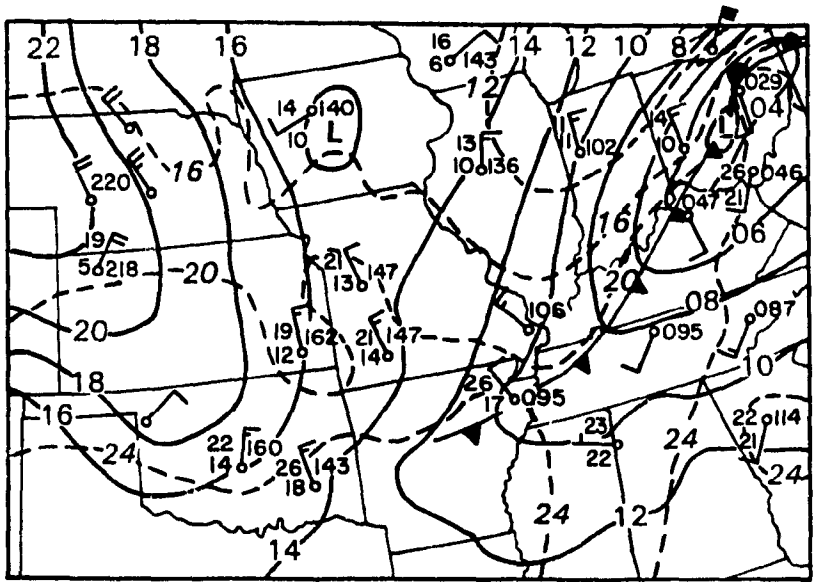

b)

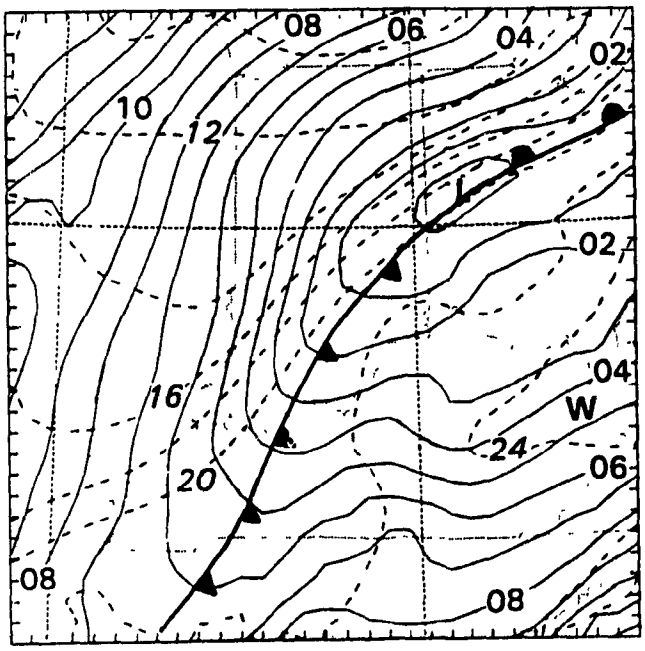

Fig. 3.6 As in Fig. 3.2 but for 0000 UTC 12 June.

a)

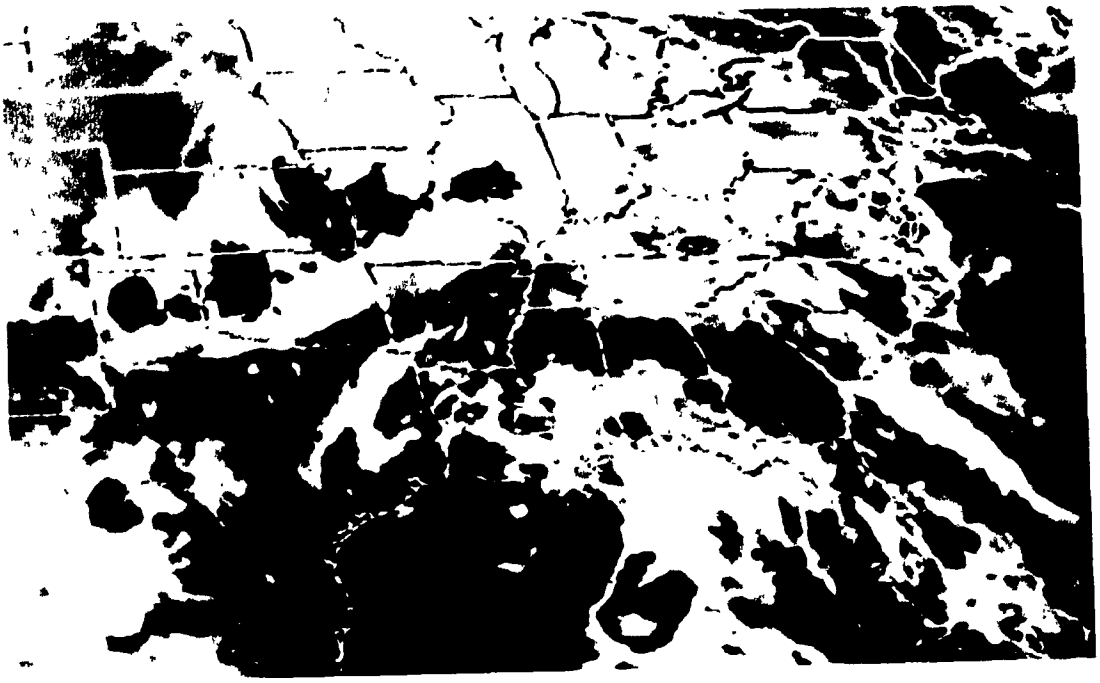

b)

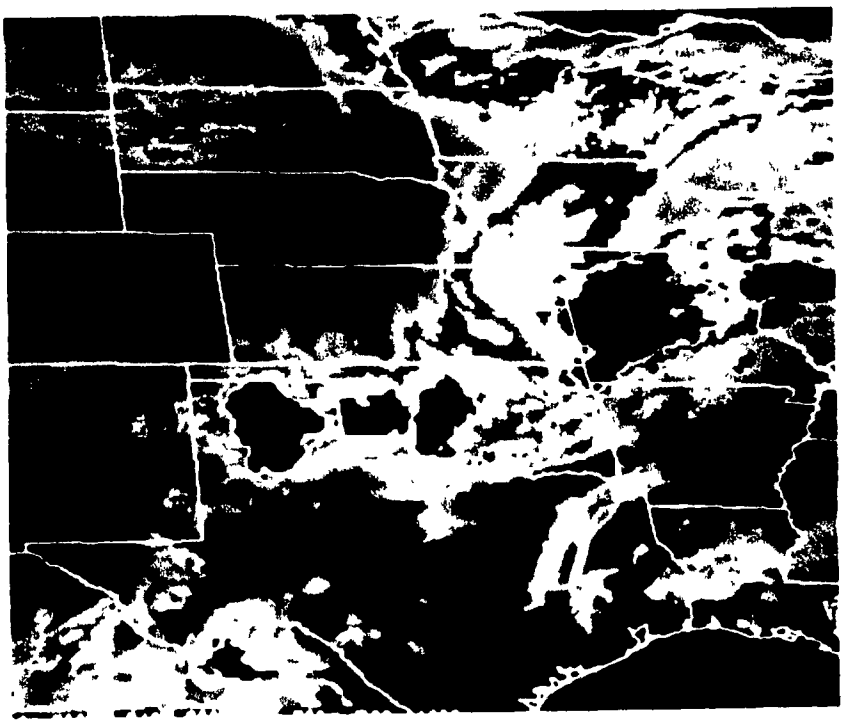

Fig. 3.7 Enhanced infrared geostationary satellite imagery at (a) 0630 UTC; (b) 0800 UTC; (c) 1201 UTC; (d) 1801 UTC 11 June and (e) 0000 UTC 12 June 1985.

c)

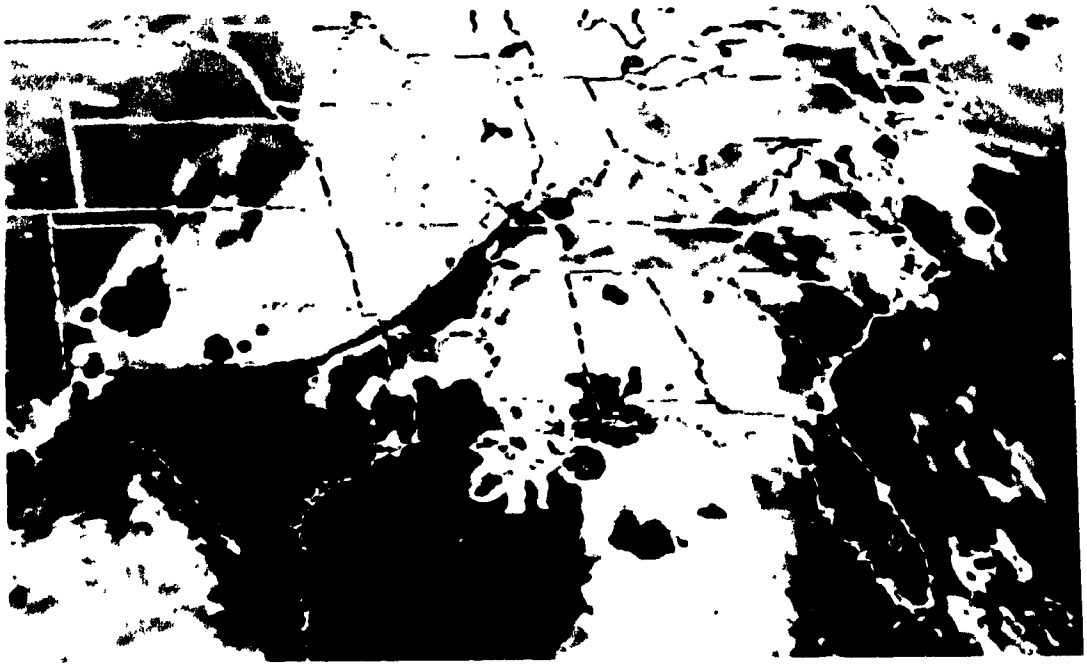

d)

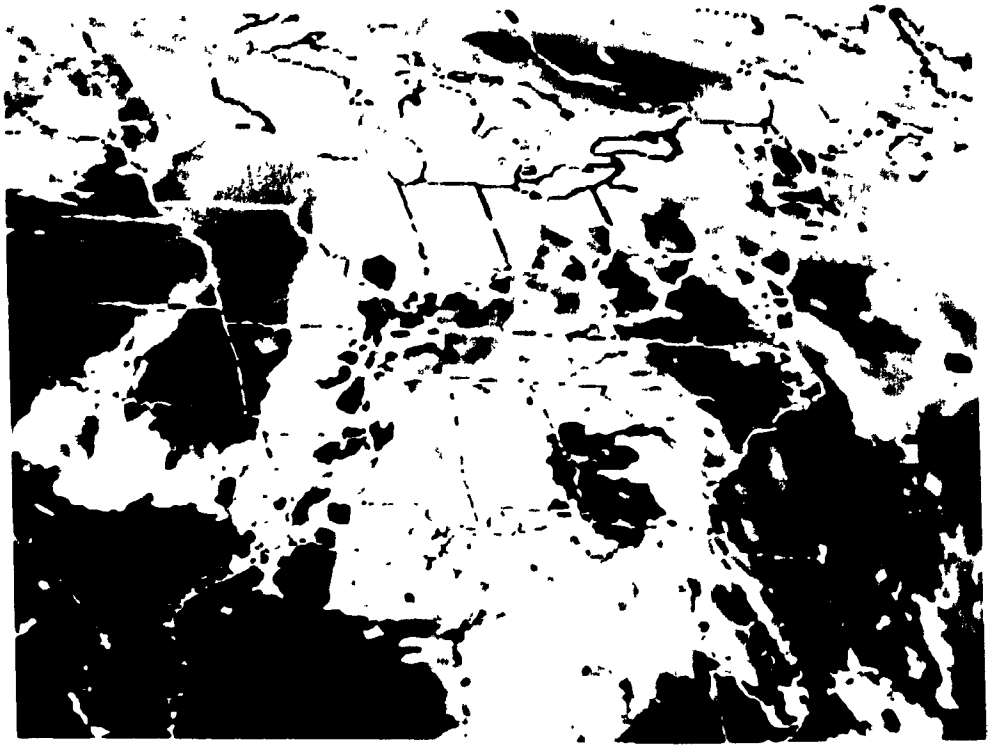

Fig. 3.7 (*Continued*)

e)

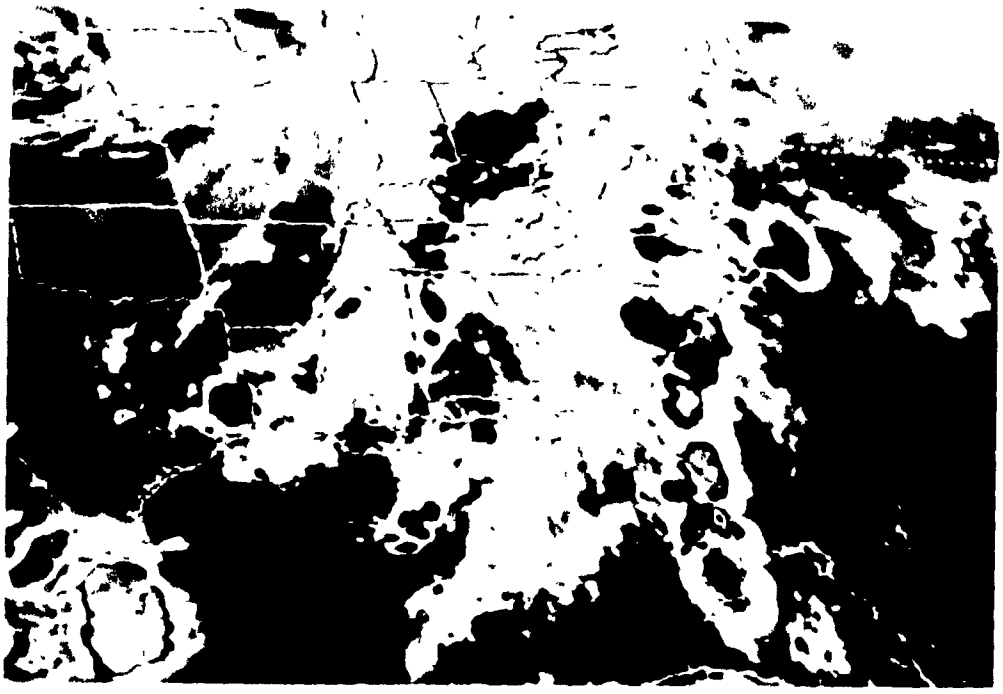

Fig. 3.7 (*Continued*)

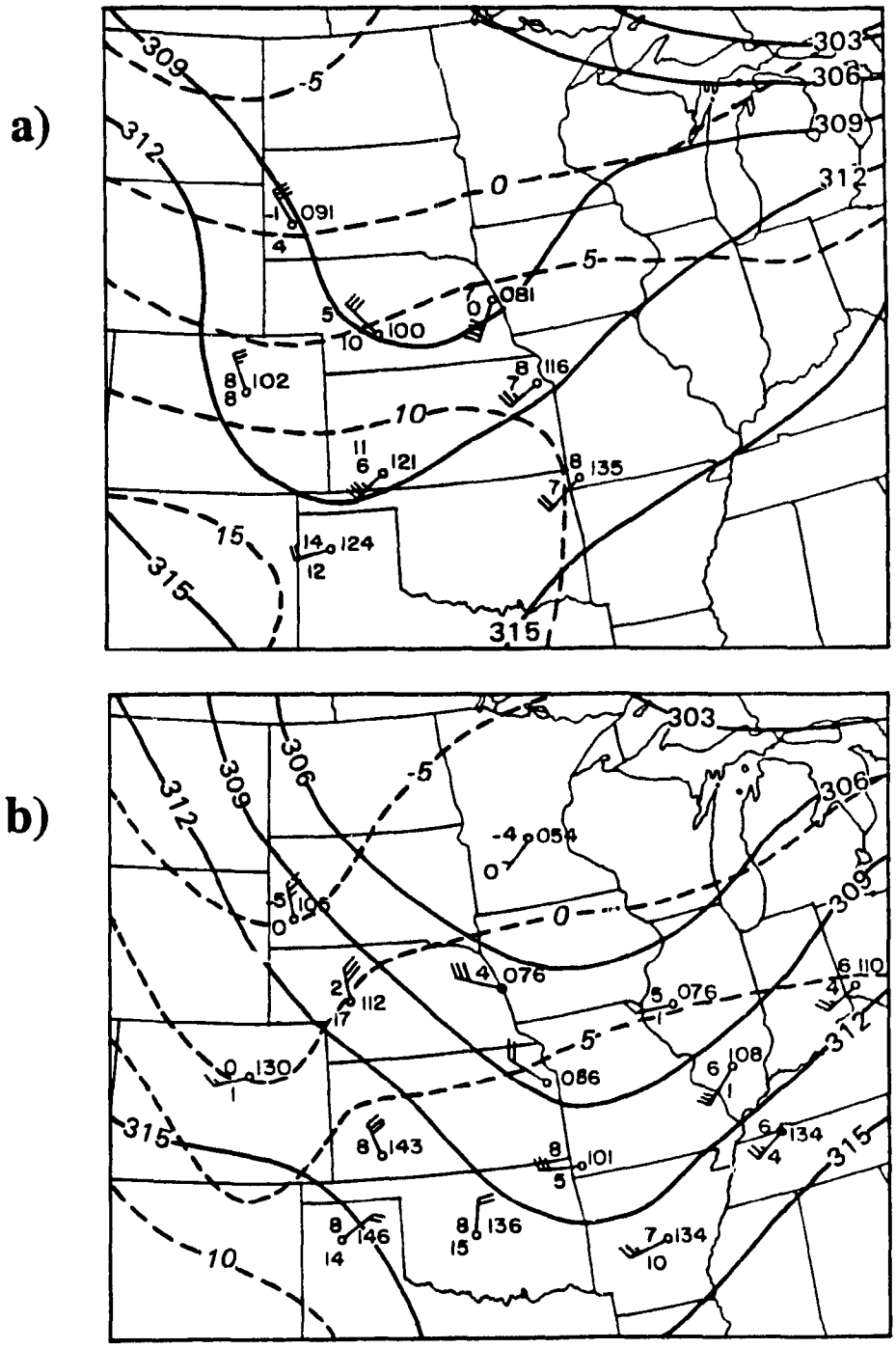

Fig. 3.8 As in Fig. 2.3 but for (a) 0000; (b) 1200 UTC 11 June and (c) 0000 UTC 12 June 1985.

c)

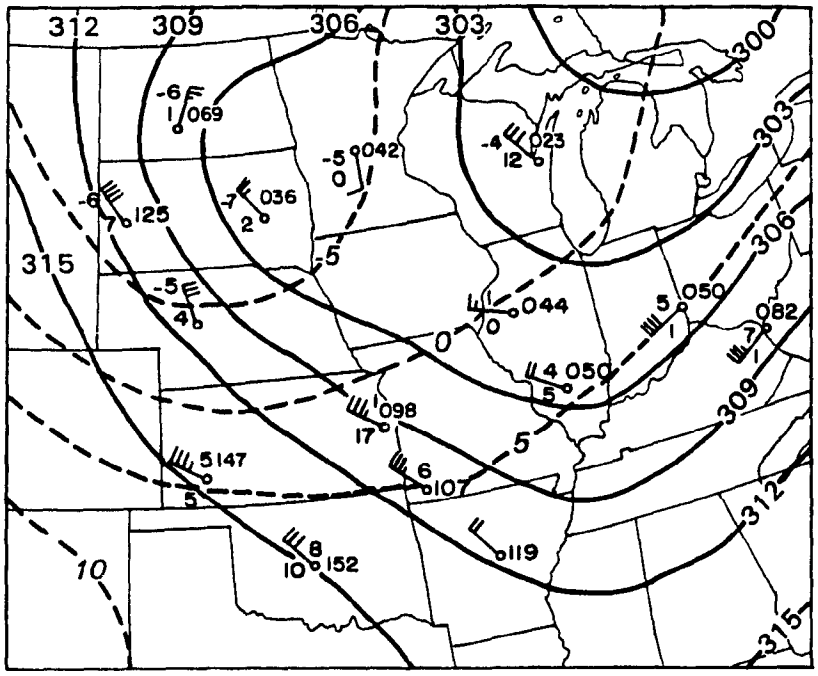

Fig. 3.8 (*Continued*)

In the following 12-h period, the squall line went through its complete life cycle, as we have seen in the last section. The large-scale flow has undergone significant changes during this period. First, the height wave deepened markedly, leading to a stronger height gradient along the trough axis (see Fig. 3.8b). Second and more importantly, the height wave propagated *in pace* with the squall system, whereas the thermal wave *remained practically at the same position* as that 12 hours earlier. These different speeds of propagation resulted in a *phase lag* between the height wave and thermal wave. According to baroclinic theory, this phase lag is instrumental in the baroclinic conversion of available potential energy to kinetic energy, and thus it is favorable for surface cyclogenesis. Third, the horizontal extent of the midlevel short-wave trough appeared to expand substantially. However, this expansion did not seem to be attributable to the development of the squall system, since it occurred much farther to the northwest and upstream of the system. Rather, this change of wavelength was more related to an incoming upper-level wave from the northwest, as will be shown in the next chapter. The thermal wave had also intensified significantly during this period. Since the thermal wave remained far behind the convective system, its intensification likely resulted from increased cold advection behind the pressure trough axis. The above results strongly suggest that the squall system had a significant impact on the evolution of the midlevel short wave, but *not* of the thermal wave. This difference in the degree to which the squall line influenced the large-scale environment will prove to be crucial in the subsequent surface development of the cyclone, as will be shown later.

At 0000 UTC 12 June, the height trough had further amplified as it propagated eastward to reach a position extending from northeastern Illinois to Mississippi (see Fig. 3.8c). The thermal trough had also intensified significantly; but it moved approximately the same distance, i.e., about 350 km for both. Thus, the phase lag between the pressure and thermal troughs remained more or less unaltered after the dissipation of the squall

a)

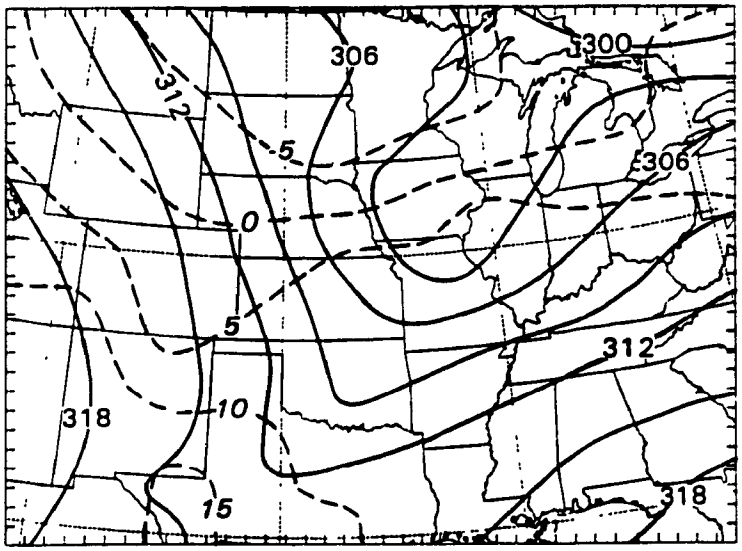

b)

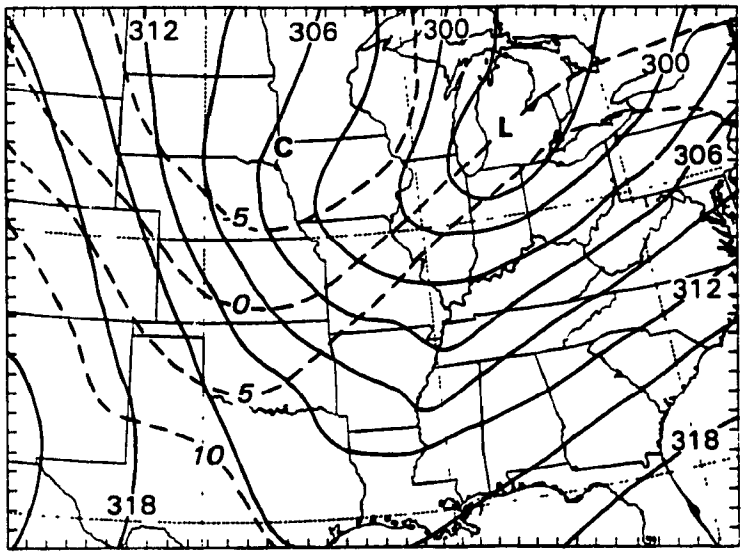

Fig. 3.9 Temperatures (°C, dashed lines) and geopotential heights (dam, solid lines) at the 700 hPa surface for (a) 24 h and (b) 36 h into the simulation. Contours identical to Fig. 2.3.

system. This further indicates the potential importance of the squall system in the intensification of the baroclinic wave and in the generation of the phase lag. This importance is clearly evidenced by comparing the large-scale flow between 1200 UTC 10 June and 0000 UTC 12 June (cf. Figs. 2.3 and 3.8c), namely, the wind speeds behind the trough axis had nearly doubled, and the phase lag between the pressure and thermal wave was markedly larger.

Fig. 3.9 shows the same fields from the 24- and 36-h simulations, valid at 1200 UTC 11 June and 0000 UTC 12 June, respectively. As can be seen, the model reproduces well the intensification of the height and thermal waves and the phase lag between them. In fact, the effects of the squall system on the structure and evolution of the height wave are more apparent in the simulation. At the end of the 36-h simulation, these two waves arrive at positions with intensity and orientations similar to the observed.

The conclusions we have reached from the behaviour of the 700 hPa flow must be considered with care, however, since this level is very close to the highest topography of the model domain (i.e, the Rocky Mountains). Therefore, it is worthwhile to check if similar characteristics could be found at higher levels, say, 600 hPa. It is evident from Fig. 3.10 that the same sequence of events were also reproduced at 600 hPa, such as the acceleration of the height trough between 12 and 24 hours into the simulation, concurrent phase lag production, and the marked intensification of the height and thermal waves at 36 h.

Finally, to further illustrate the potential significance of the squall line on the large-scale flow, Fig. 3.11 shows the accumulated model precipitation during the squall period (9-24h) and the post-squall period (24-36h), from the explicit (dashed lines) and convective (solid lines) schemes. Since ZGP showed that the model-simulated rainfall magnitude and distribution during the first 18 h compare favorably to JH88's analysis, we should believe that the simulated rainfall during and after the dissipation of the squall system would not depart significantly from the observed. Thus, only the simulated rainfall

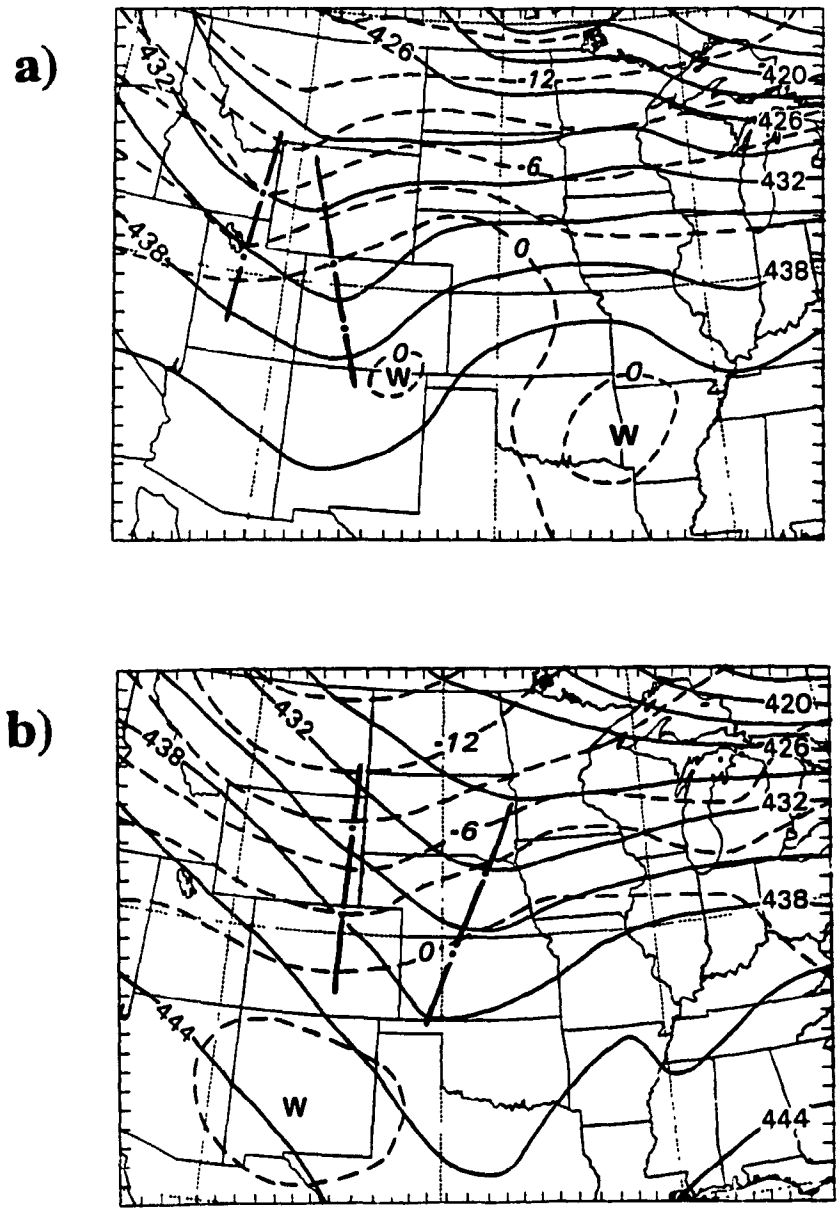

Fig. 3.10 Distribution of 600 hPa geopotential at intervals of 3 dam, and temperature at intervals of 3 °C, for (a) model initial time (1200 UTC 10 June 1985); (b) 12 h; (c) 24 h and (d) 36 h simulation. Geopotential and temperature troughs are indicated by dot-dashed lines.

c)

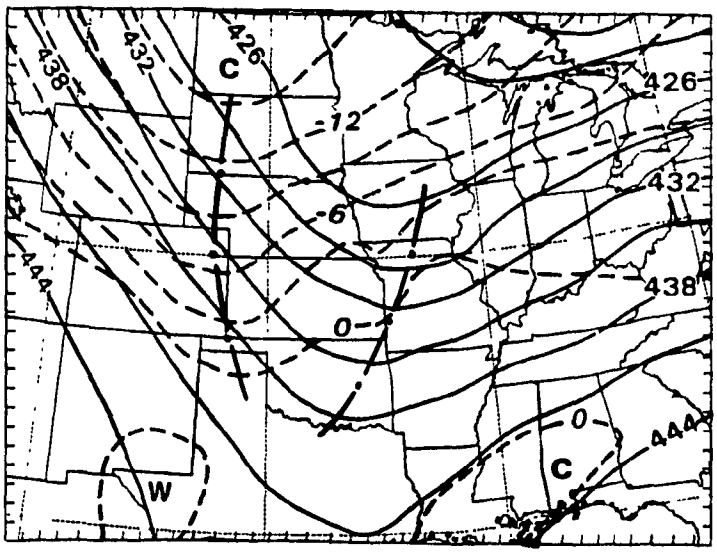

d)

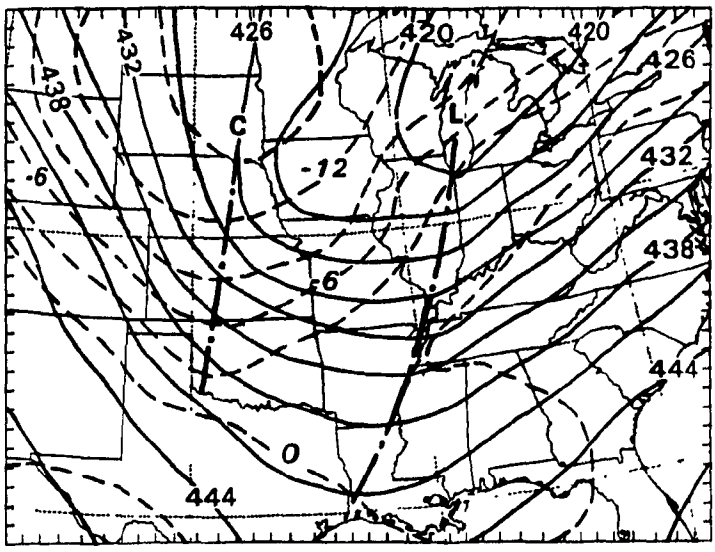

Fig. 3.10 (*Continued*)

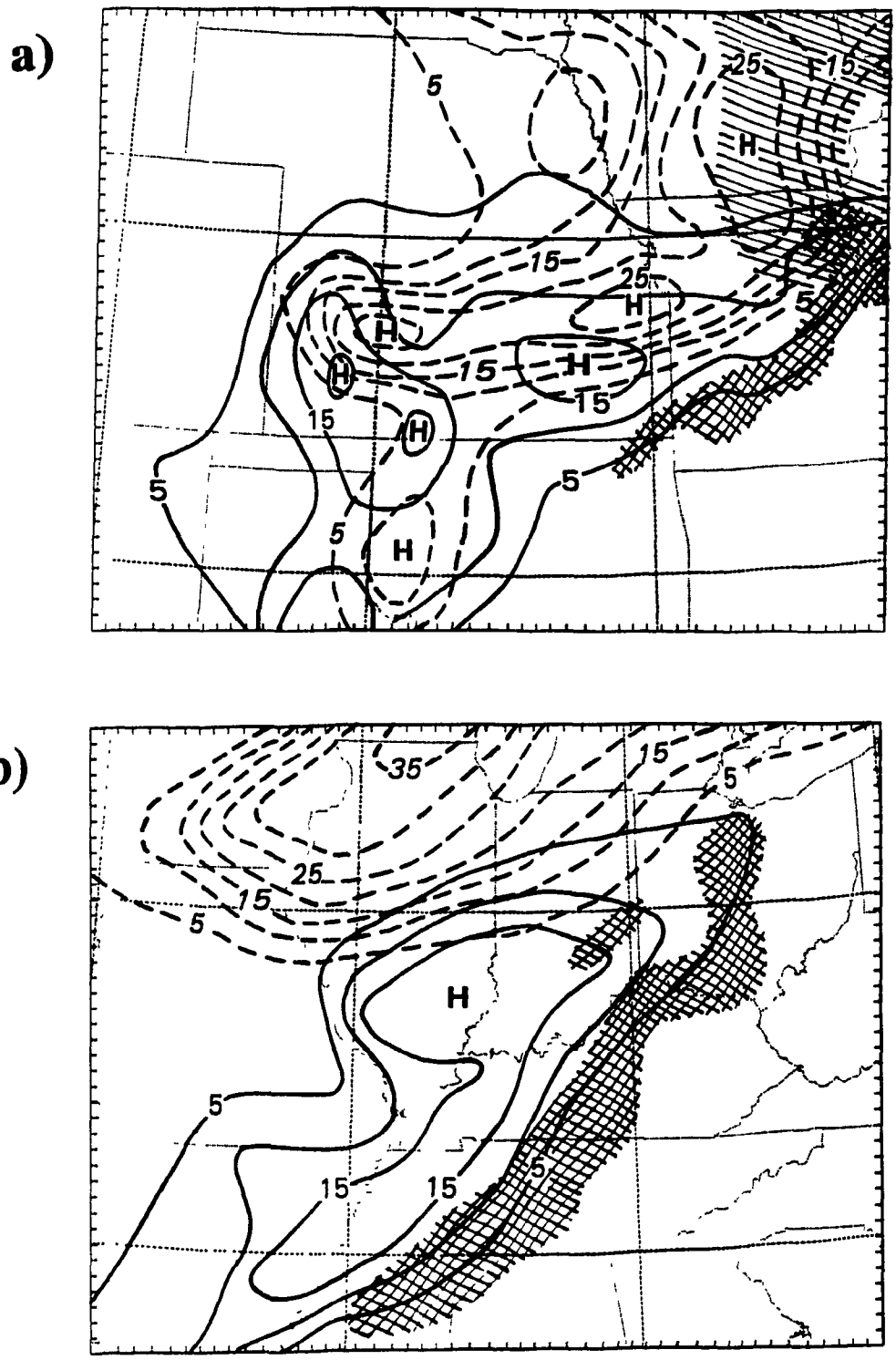

Fig. 3.11 Accumulated convective (solid lines) and grid-scale (dashed lines) model precipitation for (a) 9-24 h, and (b) 24-36 h simulation period, at intervals of 5 mm. Convective and grid-scale precipitation rates above 5 mm h^{-1} at the end of each period are indicated by cross-hatching and hatching, respectively.

information is used here to infer the importance of latent heating. It is evident from Fig. 3.11a that the grid-scale precipitation dominated over the convective throughout the lifetime of the squall line; it has two centers of more than 25 mm accumulated across Kansas. Note that since the grid-scale rainfall is generated in the FTR ascending flow, it includes precipitation from both the leading convective region and the trailing stratiform region. Note also that most of the precipitation associated with the squall system is confined to the states of Kansas and Oklahoma, particularly for the convective rainfall. As the squall system decays and moves out of the network, the convective rainfall decreases rapidly, while the grid-scale precipitation increases slightly because of more moisture content being transported northward in the southerly current. Thus, an area of over 25 mm accumulated rainfall is distributed over southern Iowa. This increase of the grid-scale precipitation coincides with the more rapid spin-up of the surface cyclone as it is merged with the wake low. A similar onset of light rain was also reported by several stations near the center of the cyclone at 1200 UTC 11 June (not shown). By comparison, the precipitation structure in the 12 h that followed the dissipation of the squall line (Fig. 3.11b) is dominated by large-scale forcing associated with the cyclone. In particular, the line of convection is associated with the cold front, while the extensive stratiform region to the north is evidently linked to large-scale ascent north of the low, as is characteristic of baroclinic disturbances.

Chapter 4 — Effects of the squall line and large-scale baroclinity

It is evident from the results presented in Chapter 3 that both the squall system and the pre-existing large-scale baroclinity have played important but different roles in the subsequent surface cyclogenesis. Thus, in this chapter we will examine to what extent these two different processes contribute to the genesis of the surface cyclone. We will first provide a review of the previous studies on the effects of latent heating on cyclogenesis and determine if the surface cyclogenesis in the present case could be clarified with the existing knowledge. Then we will investigate separately the effects of the squall system vs. large-scale baroclinity on the surface cyclogenesis, and examine their three-dimensional structures.

4.1 Previous studies

Considerable research effort has been devoted in the past to the understanding of the effects of latent heating on extratropical cyclogenesis. The earliest study could be traced back to the Nineteenth Century, when the first mechanism proposed to explain midlatitude cyclogenesis was latent heat released from precipitation near the center of storms (see Kutzbach 1979 for a review). Prevailing thought then shifted from this essentially thermal origin of cyclones to a more dynamical one, with succession of the pioneering work of Margules (1903) on the dry energetics of storms to the creation of the famous Bergen School of cyclones in the 1920s, and to the breakthrough of baroclinic theory by Charney (1947) and Eady (1949). According to the theory, strong temperature gradients, low static stability, a phase lag between the mass and wind fields and a preferred wavelength are the necessary conditions for baroclinic development.

The interests in the latent heating effects were revived in the 1950s with the introduction of numerical weather prediction models. Earlier numerical studies, such as Aubert (1957) and Danard (1964, 1966), used quasi-geostrophic models to examine the importance of latent heating on cyclone-scale motions. These studies demonstrated that latent heating from precipitation tends to increase the upper-level and decrease the lower-level height of isobaric surfaces, thereby leading to the deepening of cyclones and acceleration of their movement. The deepening of cyclones was shown to be achieved through production of additional available potential energy and an increased rate of kinetic energy generation. Note, though, that these earlier modeling studies considered only the grid-scale (> 100 km) condensation. The growing attention was paid to the roles of cumulus convection on extratropical cyclogenesis after Riehl and Malkus (1961), Charney and Eliassen (1964) and Kuo (1965) established the importance of cumulus convection in the development of tropical disturbances. For example, Tracton (1973) and Bosart (1981) argued that cumulus convection in the vicinity of the cyclone center could play a crucial part in the rapid intensification and even in the initiation of cyclones. Gyakum (1983) showed evidence to suggest that the extreme development of the Queen Elizabeth II cyclone was a result of the latent heat release in organized cumulus convection. Results of Tracton (1973) and Gyakum (1983) also exhibited greater deepening rates when a higher proportion of convective heating was released in the lower troposphere. These results have significant implications with respect to the relative importance of convective vs. stratiform precipitation in surface cyclogenesis. This is because stratiform precipitation generally produces a heating maximum at a relatively lower level than cumulus convection, thus being more favorable for cyclogenesis. This has been later confirmed by numerical simulations of Anthes and Keyser (1979), Anthes et al. (1983) and others in which both cumulus parameterization and grid-scale condensation were implemented.

A number of more recent studies have stressed that the impact of diabatic heating on cyclogenesis, whether it be stratiform or convective in nature, should be viewed as a nonlinear problem rather than a simple linear addition to dry dynamics (e.g., Smith et al. 1984; Uccellini et al. 1987; Pauley and Smith 1988; Kuo et al. 1991). Attempts at gaining more physical insight into this nonlinearity have also been made, with the isentropic potential vorticity (IPV) perspective (Hoskins et al. 1985; Davis and Emanuel 1991), to isolate the effects of non-conservative processes on dry dynamics. Latent heating in the ascending flow will increase the magnitude of IPV below and decrease it above, thereby enhancing the low-level cyclonic circulation. However, a recent study by Davis et al. (1993) shows that such a superposition of positive IPV onto the dry dynamics does not alter the basic development mechanism of cyclones. In other words, these systems are baroclinically driven in nature and they are only modulated by diabatic heating.

Despite the considerable research interests in extratropical cyclones, a majority of these studies only focused on rapidly deepening storms that occurred during the cold season or over oceans. Little attention has been paid to extratropical cyclones that developed within weak baroclinic environments or during the growing season. However, a growing number of studies on mesocyclones, that developed during the summertime, have appeared in the recent literature (e.g., Houze 1977; Zhang and Fritsch 1987, 1988; Brandes 1990; Bartels and Maddox 1991; Johnson and Bartels 1992; Zhang 1992). In contrast to the baroclinic systems discussed above, these mesocyclones, ranging from 50 to 500 km, are convectively driven in nature and mostly associated with organized MCSs. Zhang and Fritsch (1988a) and Zhang (1992) have provided extensive discussions on the mechanisms of mesocyclogenesis: one could be induced by low- to midlevel latent heat release in mesoscale ascent (Bosart and Sanders 1981; Zhang and Fritsch 1988b; Menard and Fritsch 1989), and the other induced by mid- to upper-level diabatic cooling in mesoscale descent (Brandes 1990; Biggerstaff and Houze 1991b; Zhang 1992). For a warming-induced

mesocyclone, a midlevel warm-core structure is expected when latent heating exceeds upward adiabatic cooling, and the cyclonic circulation will be maintained through the thermal wind relationship. By comparison, a cooling-induced mesocyclone is characterized by diabatic cooling above and adiabatic warming below, so its genesis occurs initially through tilting of horizontal vorticity associated with vertical shear and later enhanced by vortex stretching. These results have led Zhang (1992) to conclude that low-to-midlevel mesocyclones may be the basic dynamic effects of MCSs on their larger-scale environments, since they can be induced by either latent heating (in mesoscale ascent) or cooling (in mesoscale descent).

Apparently, the previous studies of cyclogenesis have focused on either large-scale baroclinically-driven or mesoscale convectively-driven systems. In the present case, the surface cyclogenesis occurred clearly as a result of the strong interaction between the squall system and large-scale baroclinity. Specifically, the present squall line was initiated by baroclinic forcing, and then the surface cyclogenesis did not take place until *after* the dissipation of the MCS. This scenario raises several interesting questions. For example, would the surface cyclogenesis occur without the development of the squall system? If the role of the squall system was crucial, why didn't the genesis take place in pace with the squall's intensification? Or if both the large-scale baroclinity and squall system were equally important, how did they interact with each other? and to what extent do they contribute individually to the cyclogenesis? Furthermore, it has been shown that the midlevel short wave in the present case propagated much faster than the thermal wave, resulting in a phase lag more favorable for cyclogenesis. Thus, what processes are involved in the development of such a phase lag? since this phenomenon has not been explored in previous studies.

4.2 Individual roles of moist convection and large-scale processes

We have shown in Chapter 3 that, in spite of minor differences, the model performed extremely well in reproducing the observations, particularly the key events of the squall line dissipation and the subsequent surface cyclogenesis. Therefore we should be confident that the model simulation can be used to provide a deeper understanding of the dynamical processes leading to the surface cyclogenesis.

To isolate the effects of large-scale baroclinity on the surface cyclogenesis, a sensitivity simulation was conducted ("dry" run), in which neither convective nor grid-scale condensation were included, while keeping all the other physical parameters identical to the control run ("moist" run). Without the forcing from the diabatic heating, the model atmospheric circulations were only dominated by advective processes. This presumably represents the "true" evolution of the large-scale environment without the influence of the squall system. The simulation will also help reveal whether or not the pressure perturbations and low-to-midlevel baroclinity at the model initial time would lead to the surface cyclogenesis at the end of the 36-h integration. Comparisons between "dry" and "moist" runs will also provide insight into the effects of the squall system on the surface cyclones.

a) Effect of the large-scale baroclinicity

Fig. 4.1 shows the large-scale perspective of 36-h simulated sea-level pressure and 1000-600 hPa thickness from the "dry" run, as compared to that from the "moist" run. Of particular interest is that in spite of no latent heating a surface cyclone has also developed at the end of the 36 h integration. As shown in Zhang and Gao (1989, see their Fig. 18), there is little evidence on the development of organized cyclonic circulation even up to 18 h into the simulation. Only a pressure trough is located ahead of the surface cold front; but its central pressure has decreased from 1009 to 1005 hPa during the first 18 hours. The surface

a)

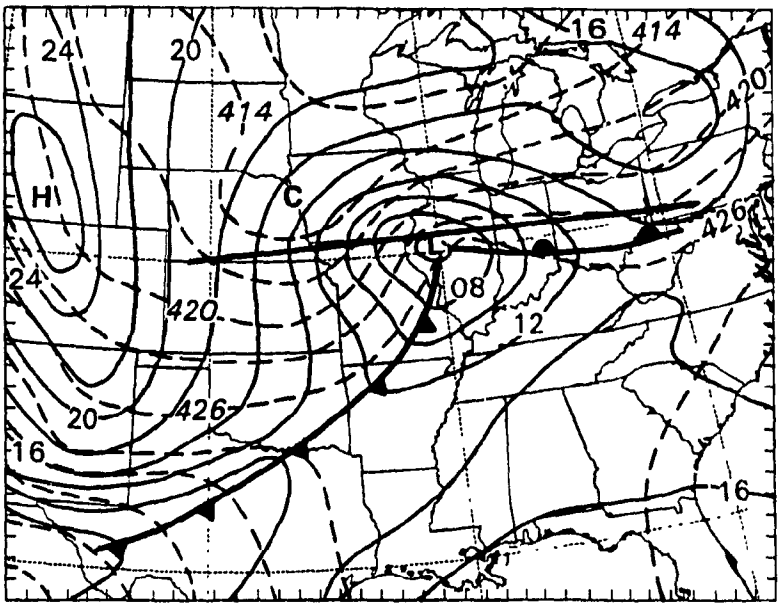

b)

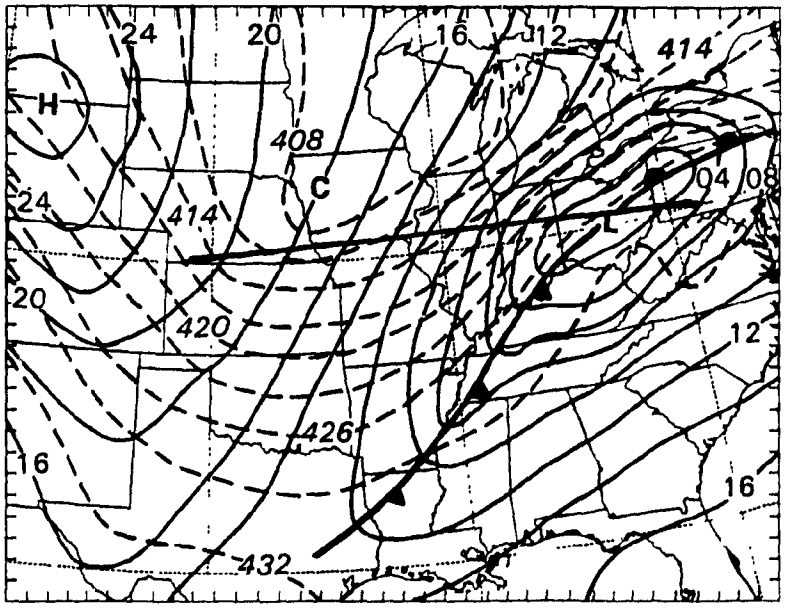

Fig. 4.1 Distribution of sea-level pressure (solid lines) at intervals of 2 hPa, and 1000-600 hPa thicknesses (dashed lines) at intervals of 3 dam, from (a) 36 h "dry" run and (b) 36 h "moist" run. Heavy solid lines denote the position of cross-sections used in Figs. 4.3, 4.4 and 4.5. Pressures labeled as in Figs. 3.1-6.

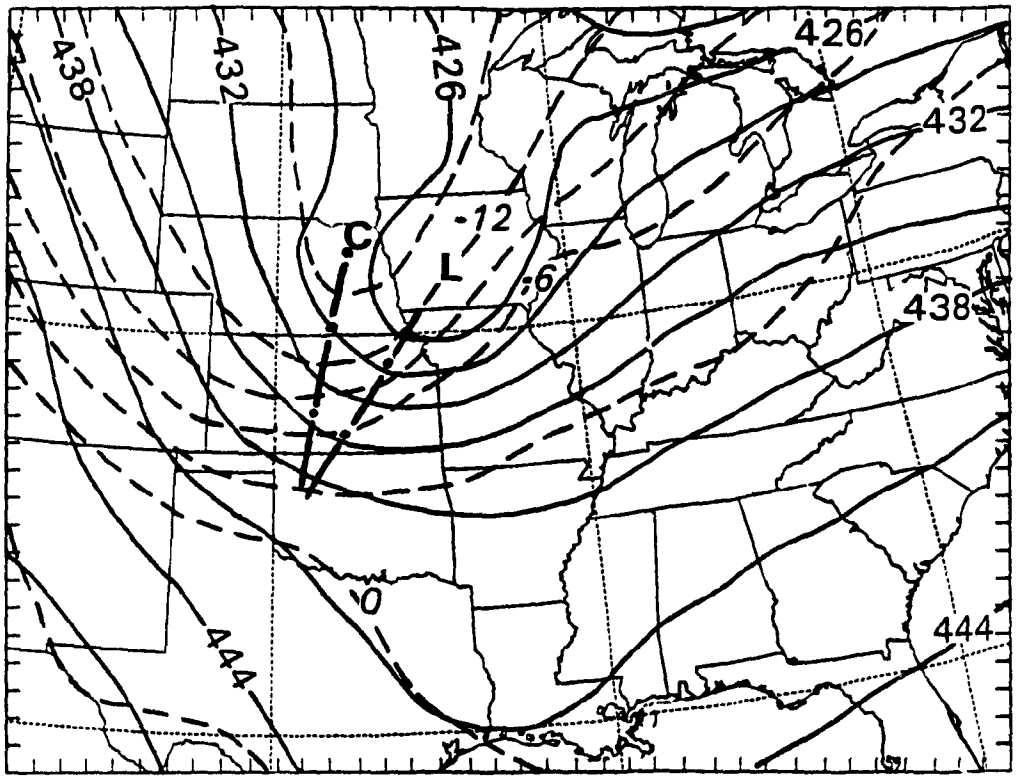

Fig. 4.2 As in Fig. 3.10d but for "dry" run.

pressure pattern does not become cyclonically organized until after 21 h into the simulation, but with little changes in intensity thereafter. Perhaps such a sequence of the cyclonic evolution should be expected when considering the interaction of a cold front with a high topography (i.e., the Rocky Mountains). Specifically, the initial phase lag between the height and thermal waves (see Fig. 2.3) would lead to the intensification of the low that is originally located over western Nebraska at 1200 UTC 10 June, if there were no topography. The organized surface cyclone fails to develop in the first 18 hours, because the large-scale baroclinicity is relatively weak and it may be overpowered by the topographical forcing, as the cold front accelerates downslope of the high plateau. The system then becomes more dictated by baroclinic theory as it moves far away from the Rocky Mountains. However, the occurrence of little deepening during the second 18-h period suggests that there may be little available potential energy for kinetic energy production. The distribution of 600-hPa height and temperature structures, as given in Fig. 4.2, shows that this is indeed the case. Namely, very little phase lag is present at the end of 36-h simulation, as compared to that at the model initial time. It follows that the initial short wave and the cold advection behind it, though weak and shallow, have some impact on the genesis of the present surface cyclone, and the genesis processes tend to reduce the phase lag between the height and thermal waves, as predicted by baroclinic theory.

b) Effect of moist convection

Now let us examine the effects of including latent heat release or the squall system on the surface cyclogenesis. Several differences between the "moist" and "dry" runs can be immediately seen by comparing Fig. 4.1a and 4.1b. First, the surface cyclone in the presence of the squall system moves much faster than the "dry" one. The difference in position is about 750 km by the end of the 36-h integration. The slower movement in the absence of latent heat release has also been noted by Aubert (1957) and Kuo et al. (1991) in association with more rapidly deepening surface cyclones. Second, the surface low in the

presence of the squall-line convection is 5 hPa deeper, a phenomenon that has been found in many of the previous studies. Third, the spatial scale of the "moist" cyclone is much greater, notably along the NE-SW direction, than that of the "dry" one. The greater extent implies the larger inertial of the circulation and more kinetic energy content associated with the perturbation. In other words, more rapid deepening of the "moist" cyclone could be expected if its horizontal extent were similar to the "dry" cyclone. Fourth and perhaps more significantly, including the squall system results in a marked increase of large-scale baroclinicity in the lower half of the troposphere. As shown in Fig. 4.1, the 1000-600 hPa thickness gradients between the leading edge of the cold front and the coldest point (i.e., the point 'C') are about 210 m and 120 m, respectively, in the "moist" and "dry" runs. The 90 m difference in thickness represents an increase of a 6 K mean-temperature gradient across that distance in the lower troposphere. This is clearly a pronounced contribution of deep convection to the large-scale environment and one of the important factors in explaining the more rapid development of the "moist" cyclone.

While the thickness gradient in the "moist" run is nearly twice as large as that in the "dry" run, the positions of the thickness troughs in these two simulations are very similar, namely, they are oriented roughly from eastern Nebraska to northern Texas. A similar situation also occurs with the 600 hPa thermal waves in these two runs (cf. Figs. 3.10d and 4.2). This implies that the propagation of the thermal wave is primarily governed by large-scale or adiabatic processes, in spite of the substantial enhancement of baroclinicity by moist convection.

Note that the thickness trough axes also lag behind the closed surface cyclones in both simulations, a typical characteristic of baroclinic systems (see Holton 1979). However, the lag in the presence of convection, as also appeared in midlevels, is much greater. As have been demonstrated by previous studies (e.g., Aubert 1957; Chang et al. 1982), organized latent heat release will result in pressure falls below the level of maximum heating and pressure rises aloft. In the present case, the tremendous amount of net warming

(cooling) associated with the FTR (RTF) flow, as shown in Zhang and Gao (1989, see their Fig. 20), would produce midlevel pressure deficits on the scale of the squall system, thereby enhancing the midlevel short wave and forcing it to propagate with the system. This feature has also been noted in other case studies, e.g., by Zhang and Fritsch (1986, 1988a). In fact, we have seen in Chapter 3 that the movement of the midlevel short wave coincides with the evolution of the squall's cloud shields. Furthermore, Zhang and Gao (1989) have shown that the squall system propagates much slower when the parameterized downdrafts in the FC scheme was turned off. Apparently, the cold downdrafts associated with the parameterized convection and stratiform (grid-scale) precipitation tend to assist the MCS accelerate forward. Thus the propagation of the system is determined by the interaction between the convectively generated downdrafts and conditionally unstable environment ahead of the squall line. Then, the squall system leaves behind a bulk of cold air mass, so the baroclinicity is enhanced and spread out into a larger area more markedly in the lower layers. Since the midlevel thermal wave is basically adiabatically driven and the pressure wave is convectively driven, these two different processes would naturally result in a phase lag between the two waves, as exactly occurred in the present case. Because of the phase lag, stronger cold (warm) advection occurs behind (ahead of) the trough axis in the "moist" case than that in the "dry" case (see Figs. 4.1 and 3.10d). Furthermore, as the surface cyclone deepens, the thermal wave also intensifies as a consequence of enhanced cold advection behind the trough axis, thereby creating a positive feedback between the two types of waves. These processes clearly account for the persistent deepening of the surface cyclone as it moves toward the Atlantic Ocean.

c) Interaction between moist convection and its larger-scale environment

The phase lag described above could also be considered as a product of the interaction between the squall system and the large-scale environment during the squall's life cycle. As mentioned previously, the squall line was initiated by the baroclinic forcing

associated with the cold front and midlevel short wave. However, the subsequent development of the squall system is determined by convective interaction with potentially unstable conditions in the prefrontal environment. The larger-scale baroclinic environment only provides a favorable condition for but does not control the evolution of the system. Zhang et al. (1989) showed that the squall line decays as it advances into the conditionally less unstable environment to the east of the PRE-STORM network, even though the large-scale baroclinic forcing has significantly increased. New organized convective development along the cold front and stratiform precipitation near the cyclone center do not occur until 1800 UTC June 11 (see Fig. 3.7d), when the cyclone intensifies and the daytime boundary-layer development regenerates a potentially unstable environment.

According to baroclinic theory, as long as the phase lag is present, more available potential energy will be converted to kinetic energy for cyclonic development. However, during the squall's period, the energy conversion is dominated by convectively generated circulations, such as the FTR ascending and RTF descending flows, and midlevel mesovortices. Such circulations favor the development of mesohighs and wake lows (see JH88; Zhang and Gao 1989) superposed on the larger-scale surface trough, as shown in Chapter 3. Thus, the baroclinic spin-up of the surface cyclone could not become evident until the squall system dissipates and the convectively generated perturbations are absorbed by larger-scale flow. Nevertheless, the increase in the phase lag may account for the continued expansion and slow deepening of the larger-scale surface pressure trough even during the squall's life cycle.

While the cyclonic development mechanism after the squall's dissipation could be viewed as being similar to that in the "dry" cyclone, it should be realized that it is the diabatic heating associated with the squall system that produces such a baroclinically favorable configuration. Furthermore, the large-scale baroclinicity has been substantially enhanced by the development of the MCS, and through its subsequent interaction with the amplified short wave. Thus we may state that the baroclinic forcing is responsible for the

initiation of deep convection along the squall line, whereas the squall system *conditions* the baroclinic environment for subsequent cyclonic development. Without the moist convection, the surface cyclone would be much weaker, have much smaller extent, and perhaps last much shorter.

d) Vertical structure of the cyclone

To further illustrate the interaction between the squall line and the large-scale baroclinity, Figs. 4.3a,b show E-W vertical cross sections of height and temperature deviations at the end of the 36-h integration from "moist" and "dry" runs, respectively. The cross sections are taken along the same line and roughly through the cyclone centers in these two simulations. All deviations are obtained by deducting their pressure-level averages in the cross section. One can see that the troughs of height deviations in both the "moist" and "dry" runs tilt westward with height, and so do the temperature troughs. This type of vertical structure is a typical characteristic of baroclinic waves. However, the westward tilt as well as the phase lag between the height and thermal troughs is much greater when convective effects are included. Furthermore, moist convection enhances substantially the large-scale baroclinicity in a deep layer of the troposphere, more significantly around the trough axis of the short wave. The convectively generated thermal gradient is as strong as 14°C/600 km up to 600 hPa. Most of the differences occur between the centers of the "moist" and "dry" cyclones. The "moist" cyclone is now displaced approximately underneath the upper-level height ridge.

To understand the *net* effects of moist convection on its larger-scale environment throughout the troposphere, Fig. 4.4 shows the height and temperature differences between the two simulations (i.e., "moist" minus "dry") along the same cross section as in Fig. 4.3. In general, moist convection produces net warming above the short-wave trough axis with a maximum value of >8 K occurring near 300 hPa and net cooling below with a minimum value of < -10 K occurring in the lowest layers. In particular, moist convection generates a

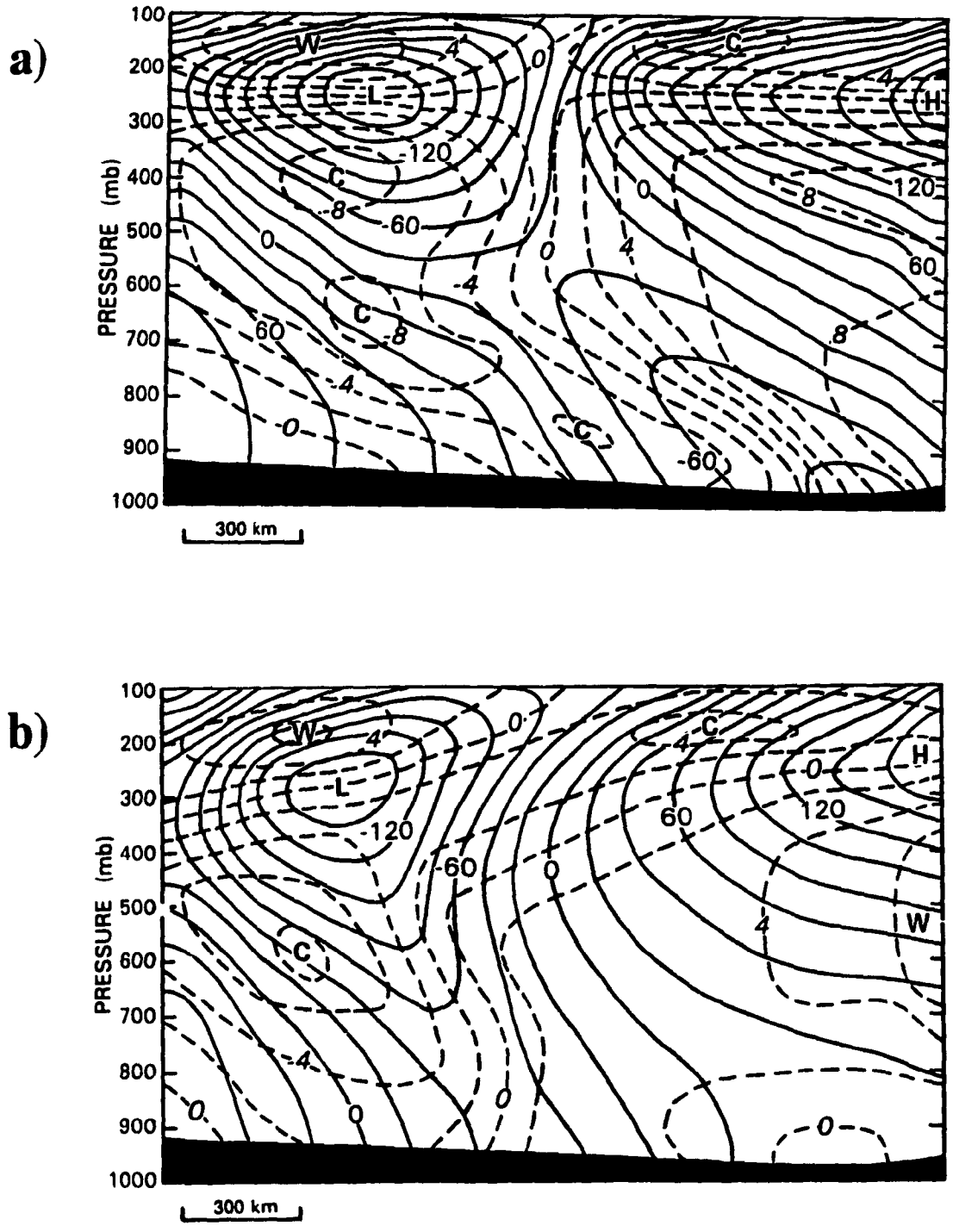

Fig. 4.3 Vertical cross-sections of height deviations (solid lines) at intervals of 20 m, and temperature deviations (dashed lines) at intervals of 2°C for (a) 36 h "moist" run and (b) 36 h "dry" run, both taken along line in Fig. 4.1. Deviations were taken from pressure-level averages along the cross-sections. West is on the left.

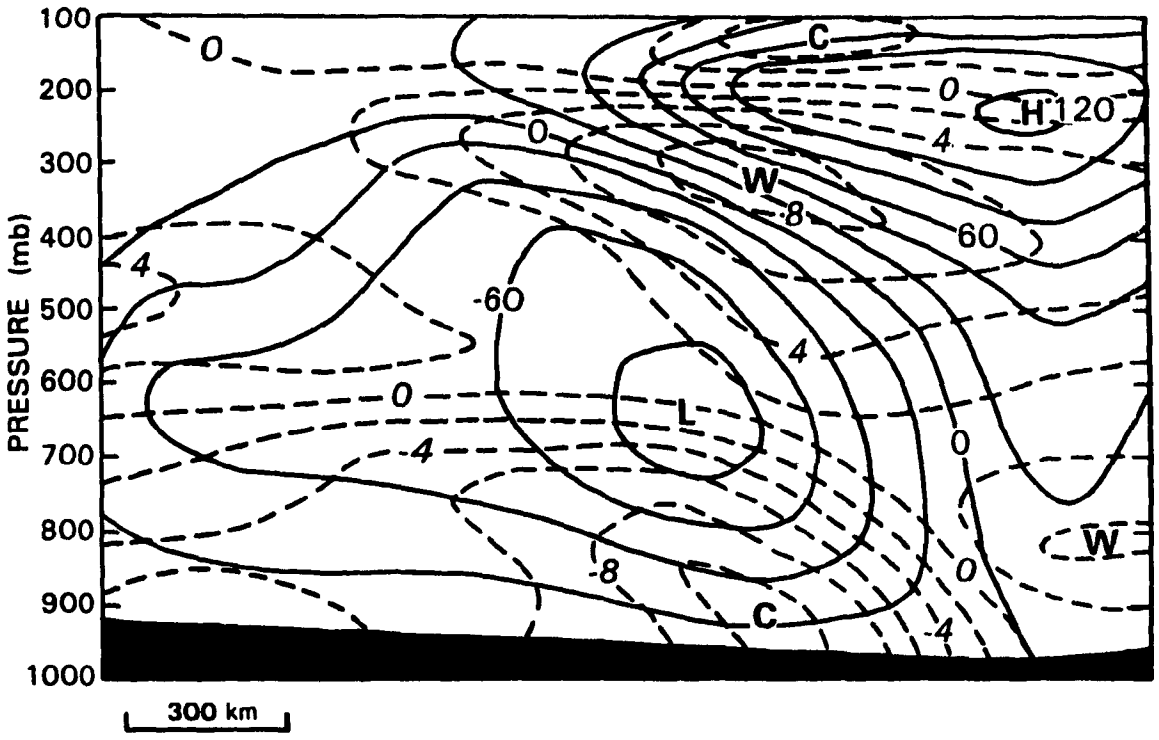

Fig. 4.4 Vertical cross-section of actual (*not* deviations) height and temperature differences between the "moist" and "dry" runs (i.e., "moist" minus "dry"), along the same line and with same contour intervals as in Fig. 4.3.

deep layer of colder air mass (up to 600 hPa) on a scale of more than 1500 km. This further indicates the importance of deep convection, through moist downdrafts, in enhancing the large-scale baroclinicity. Clearly, such strong warming and cooling over a large scale could hydrostatically produce a significant influence on the midlevel pressure wave; the net result is a height deficit of more than 80 m near 600 hPa. Diabatic heating also produces a net height rise zone throughout the troposphere over the cyclone center. Of particular interest is that, in the present case, the height deficit and rise centers are not coherently distributed in the vertical. In this sense, we should not treat the effects of latent heat release on the surface cyclogenesis as a simple linear addition to the "dry" dynamics, especially when considering the cumulative influence of moist convection in a sheared environment. Specifically, the net height rise, corresponding to a net warming column up to 200 hPa over the cyclone center, may be more associated with the immediate thermodynamic effect of latent heating, just like that associated with convectively-driven mesocyclones. The occurrence of little cooling below and localized warming near 800 hPa indicates that the grid-scale condensation is dominant over the cyclone center. In contrast, the height deficit, maximized at the top leading edge of the cold pool, is more or less dynamically generated as a result of mass evacuation as the colder air subsides. It would generally take several hours for an MCS to build such a depth of cold pool. For example, in the present case the time scale is about 8.5 hours, assuming a propagation speed of 16 m s^{-1} from the leading edge of the cool pool at the surface to the location of the midlevel low center. During this period, the large-scale circulation has been substantially altered even just through baroclinic energy conversion processes. Clearly, this nonlinear aspect of organized MCSs is closely associated with moist downdrafts, which have been ignored in previous cyclogenesis studies.

Finally, Fig. 4.5 compares the relative vorticity field from the two simulations. The cyclonic flow component concentrates roughly along the height-wave trough axis, since the flow has been nearly balanced with the mass field at the end of the 36-h integration. It is of interest that the large-scale processes in the control run still tends to produce some cyclonic

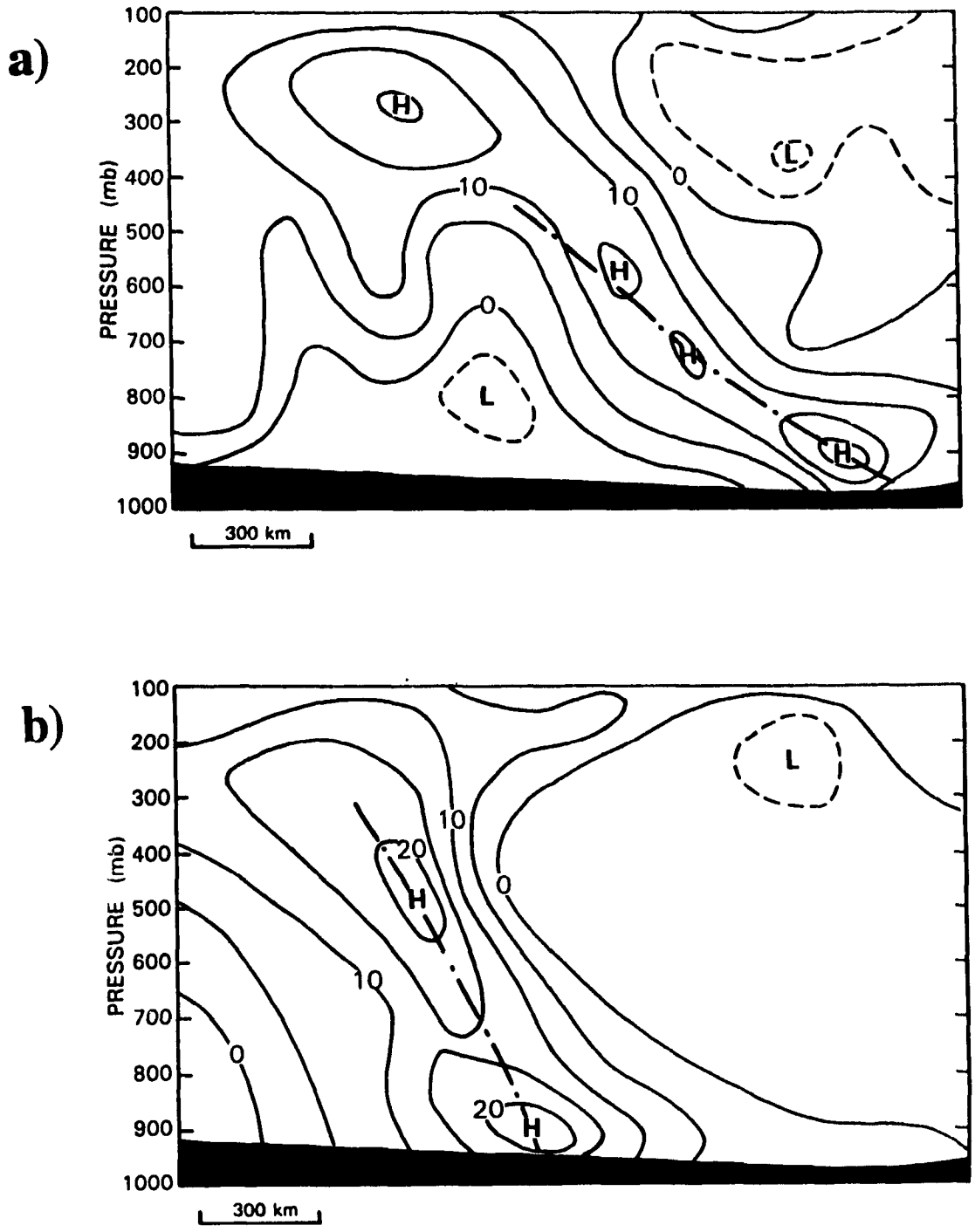

Fig. 4.5 Vertical cross-section of 36-h simulated relative vorticity at intervals of 5×10^{-5} s^{-1} from (a) the "moist" run and (b) the "dry" run, and taken along same line as in Fig. 4.3. Solid (dashed) lines represent positive (negative) values. Superposed are positions of troughs in height deviations (dot-dashed lines) as inferred from Fig. 4.3.

flow beneath the upper-level vorticity center, as does with the "dry" cyclone. The model output indicates that this feature was related to a short wave that originated over Alberta at the initial time and propagated southeastward during the 36-h period. The wave also seemed to produce an increase in the wavelength of the midlevel circulation, as mentioned in the preceding chapter. Note that the relative vorticity is maximized at the upper level (above 500 hPa) and near 900 hPa, particularly for the "moist" cyclone. This indicates that the surface cyclogenesis in the present case is much less affected by large-scale vorticity advection than other forcing, e.g., stretching and tilting. This will be discussed in the next subsection.

e) From a mesolow to a surface cyclone

So far we have discussed how the larger-scale environment evolved from weak baroclinically driven to more convectively driven and then to moderate baroclinically driven. A natural question is: how do these variations affect the evolution of the surface cyclone from a mesolow ahead of the surface cold front at the initial time, then to a pre-squall mesolow during the squall's period, and ultimately to the formation of a large-scale cyclone?

It was shown in Fig. 2.4 that a closed cyclonic circulation and a 1009 hPa low were initially located over western Nebraska. A cold front extended from the low southwestward, and a short wave trough was also present in midlevels. ZGP (see their Fig. 9) showed that, during the first 9 hours of the simulation, the mesolow traveled southeastward to western Kansas, where it interacted with a warm front and initiated deep convection. During this pre-squall period, the mesolow deepened to 1003 hPa. While part of this deepening can be attributed to the model adjustment between the mass and wind fields during the first 2-3 hours of the simulation, it was apparent that the cold front and the midlevel short-wave trough supported the surface low on its downslope trajectory from the foothills of the Rocky Mountains. Also, the large-scale cyclonic circulation remained centered around the

low, where convergence maintained upward motion above the low. As noted in §4.2, a similar but slower baroclinic development occurred in the "dry" run, indicating that the mesolow was mainly driven by adiabatic forcing in the pre-squall period. Additional forcing came from moist downdrafts produced by moderate convection along the cold front.

As the squall line initiated ahead of the surface front, it generated strong updrafts which quickly overwhelmed the weaker upward motion above the mesolow. As shown in Hoxit et al. (1976), compensating subsidence formed in the mid- to upper-levels just ahead of the squall line, and provoked reductions in surface pressure. This presumably forced the mesolow to accelerate forward, which then became a pre-squall low, driven by subsidence rather than upward motion. Meanwhile, evaporative cooling produced a squall mesohigh behind the gust front, enhancing pressure gradients between the mesohigh and the pre-squall low. The whole squall system then moved southeastward as it intensified.

Now let us examine the vertical structure of the surface cyclone following the dissipation of the squall line. Figs. 4.6a-c show northwest-southeast cross-sections of relative vorticity, superposed by flow vectors along the vertical plane, roughly through the cyclone center from 18, 24 and 30 h simulations. Also shown are the axes of height deviation troughs (dot-dashed lines). During the dissipation stage, i.e., at 18 h, there are two height troughs that tilt westward with height: one from the surface pre-squall low and the other from the wake low. A low- to mid-level mesovortex is located along the convergence zone between the FTR ascending and the RTF descending flows (see Zhang 1992). There is little cyclonic vorticity associated with both low-pressure zones. Zhang (1992) showed that the major vortex is now intensified as a result of vortex stretching along the FTR/RTF interface. Evidently, the mass field around the two low-pressure zones is not balanced with the *in-situ* winds. The two lows are still dominated by subsidence, and thus maintained through adiabatic warming.

It should be noted that the vorticity structures presented above differ somewhat from those given in Zhang (1992) because of the use of different locations along which the

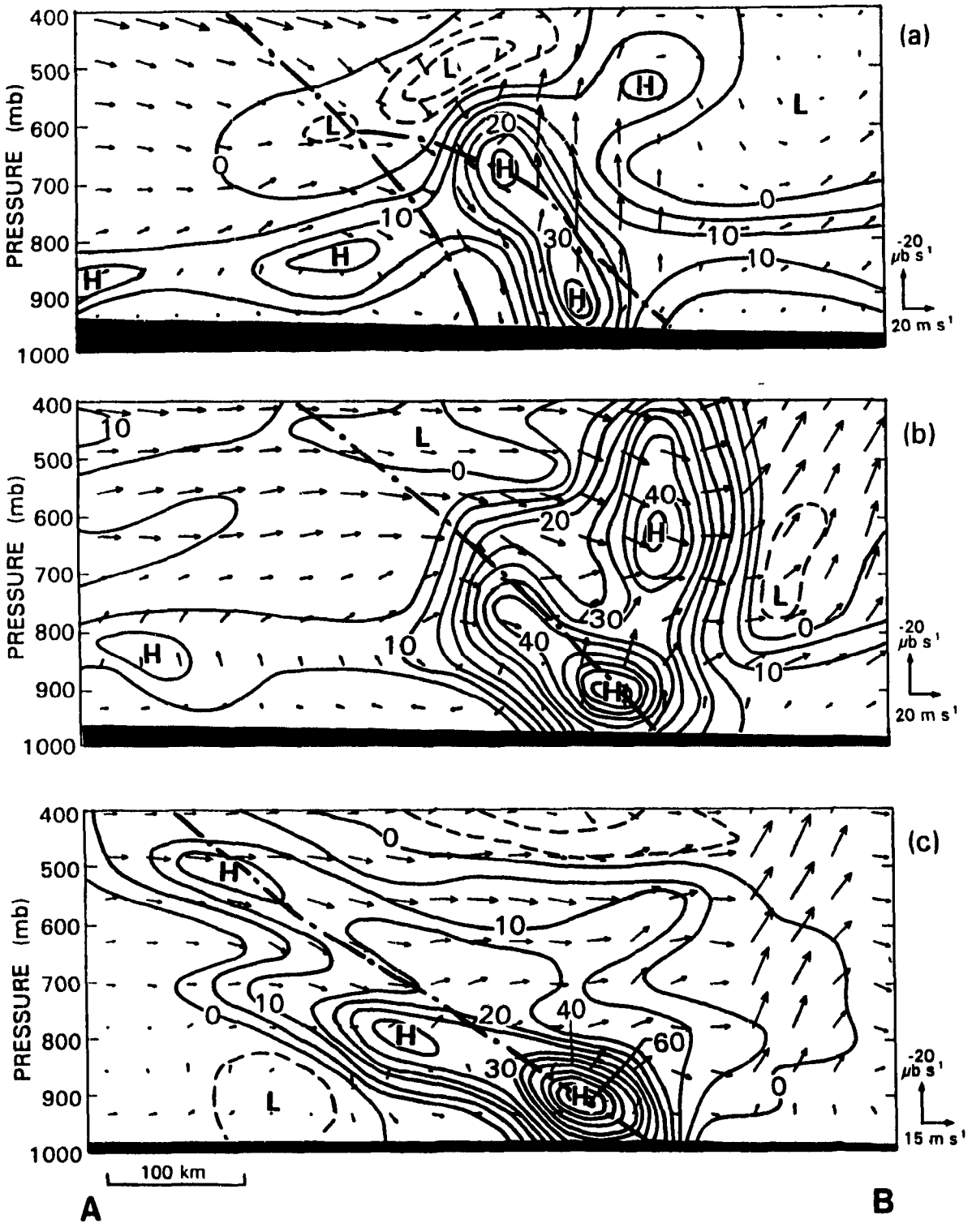

Fig. 4.6 As in Fig. 4.5, but for (a) 18 h, (b) 24 h, and (c) 30 h into the "moist" run, along lines A-B as indicated in Figs. 3.2, 3.4 and 3.5, respectively, with wind vectors projected unto the plane of the cross-sections.

vertical cross-sections are taken. It is found that the vortex center is gradually displaced downward and southeastward in the RTF descending flow as the squall system decays. Eventually, its vorticity is distributed along the leading edge of the cold pool, and thus it enhances the cross-frontal circulations as the cyclone intensifies. Therefore this mesovortex does not play a direct role in the spin-up of the surface cyclone and will not be discussed here.

At 24 h, the wake low has merged into the pre-squall low to form the surface cyclone, as discussed in Chapter 3. However, the structure of the mesovortex was altered substantially. Specifically, as the vorticity forcing decreases, the upper portion of the mesovortex is rapidly advected away from the height trough due to the presence of strong vertical shear. It is later distributed into a larger area ahead of the surface cyclone. In contrast, the near-surface vortex remains behind; but it continues to be pushed forward by the descending cold current. The vortex rapidly intensifies as it is displaced into the height trough, which corresponds to the merging of the two mesolows. Meanwhile, the wind field gradually adjusts to the mass field, as evidenced by the westward tilt of the vorticity along the height trough. Of importance at this time is a shift in the sign of vertical motion from subsidence during the squall-active period to relatively strong upward motion near the center of the surface cyclone. This strong upward motion is consistent with the more rapid cyclonic development during this stage.

At 1800 UTC 11 June (Fig. 4.6c), the baroclinic development carried on with continued spin-up of the low-level vorticity, due to the increased rate of energy conversion. The low accelerated eastward, thus reducing the slope of the height trough, along which the cyclonic vorticity is distributed. Note the persistent intense upward motion in the warm sector, further confirming the active conversion of potential into kinetic energy.

The results presented above clearly show the relative importance of deep convection vs. the large-scale baroclinity in the final intensity of the surface cyclone. The convectively generated vortices tend to enhance the cyclonic spin-up and frontal circulation after the

dissipation of the squall system. The mid- to upper-level portion of mesovortices is generally short-lived in a baroclinic environment. Thus, only the balanced portion of these mesovortices could contribute to the surface cyclogenesis. In the present case, it occurs as the mesovortex becomes in balance with the surface low that evolves from convectively driven to baroclinically driven. Without the convective effects, the baroclinic processes can only produce a weaker, smaller and short-lived surface cyclone.

Chapter 5 — Summary and concluding remarks

In this thesis, a 36-h, three-dimensional, high-resolution numerical simulation of the 10-11 June 1985 squall system has been used to investigate the impact of an MCS on large-scale surface cyclogenesis. The present study extends the 18-h simulation of the case by Zhang et al. (1989) using the same version of the PSU/NCAR mesoscale model, in which the Fritsch-Chappell (1980) convective parameterization and an explicit moisture scheme were incorporated. The model is initialized at 1200 UTC 10 June 1985 with conventional rawinsonde and surface observations, and verified against all available synoptic and mesoscale data. The model simulates very well the initiation of the squall line at nearly the right place and right time 9 hours into the simulation. A midlevel short- wave trough also assists the initiation of deep convection. The squall line then intensifies and propagates southeastward as the system's cold downdrafts interact with an unstable pre-storm environment. During the mature stage, the squall line generates typical surface pressure perturbations, such as a pre-squall low, a squall mesohigh, and wake lows, which are embedded in a weak large-scale cyclonic circulation. Also well handled by the model are a leading overturning updraft, an ascending system-relative front-to-rear (FTR) flow, and a descending rear-to-front (RTF) flow. The squall line decays rapidly after 21 hours as it advances into a more stable troposphere. During this decaying stage, the model accurately reproduces the merging of the squall's wake low with the pre-squall low, and the subsequent deepening of the merged low. After the complete dissipation of the squall system, the large-scale cyclonic circulation adjusts gradually to the resulting mass field and promotes the rapid spin-up of the surface cyclone. In addition, the squall's gust front enhances the cold front to the southwest of the cyclone and helps increase cold advection behind the cyclone. Both the observations and simulation show that the cyclone accelerates eastward and increases its horizontal extent as it intensifies baroclinically during the last 12 hours of the period.

To isolate the effects of deep convection vs. large-scale baroclinity on the surface cyclogenesis, a sensitivity simulation is conducted in which convection is turned off. By comparing this "dry" run with the control, or "moist" run, it is found that the "dry" cyclone moves much slower, has much smaller horizontal extent, and is much weaker than the "moist" cyclone. When the "moist" run is examined, the squall line modified substantially the large-scale baroclinic environment. Specifically, the abundant diabatic heating in the FTR flow tends to deepen the midlevel short-wave trough and force it to move with the squall line. In contrast, the midlevel thermal trough is driven by large-scale adiabatic processes, so it remains far behind the squall line. Thus, this leads to an increase in the *phase lag* between the height and thermal waves, as the squall system progresses eastward. Meanwhile, convectively generated cold downdrafts form an extensive cold pool of sizable depth in the cold sector of the baroclinic zone, thereby enhancing the lower tropospheric baroclinity. Thus the roles of the squall line are to *condition* the large-scale environment by enhancing the large-scale baroclinity and increasing the available potential energy. Another role of the squall line is associated with the evolution of convectively generated mesovortices. In the present case, the squall line produces a mesovortex in the convergence area along the FTR/RTF interface, and it quickly leans downshear as the system dissipates. Then, the upper portion of the vortex is advected away in the sheared flow, whereas the near-surface portion remains behind and moves into the center of the surface cyclone, thus aided in the spin-up of the surface cyclone.

The results also show strong evidence of the scale interactions of an MCS with its large-scale environment. Specifically, the initial weak baroclinity helps initiate deep convection along the squall line. Once initiated, the squall line is more or less driven by its own internal circulations. The baroclinic forcing only provides a favorable environment for the evolution of the squall system, since it is overwhelmed by convectively generated circulations. As the squall line rapidly intensifies and accelerates eastward, it enhances the large-scale baroclinity, and conditions the large-scale environment into a baroclinically more

favorable configuration. Therefore, once the convective forcing weakens, the baroclinic development mechanisms take over, leading to a more extensive and stronger surface cyclone.

It is important to point out, however, that the conclusions we have reached are based only on a single case. More case studies are needed to generalize our findings. Our results nevertheless underline the potential impact on accurately forecasting the development of MCSs in order to capture these scale interactions. This requires the use of high-grid resolution, improved initial conditions and appropriate model physics. *Failing such attempt, quantitative precipitation forecasts could be in serious error, not only for subsequent mesoscale events, but also for larger-scale systems well resolved by the model.*

REFERENCES

Anthes, R A., and D Keyser, 1979: Tests of a fine-mesh model over Europe and the United States. *Mon Wea Rev.*, **107**, 963-984.

-------, and T.T. Warner, 1978· Development of hydrostatic models suitable for air pollution and other mesometeorology studies. *Mon. Wea. Rev* , **106**, 1045-1078.

Anthes, R A.,Y -H Kuo, and J R. Gyakum, 1983· Numerical simulations of a case of explosive marine cyclogenesis *Mon Wea. Rev.*,**111**, 1174-1188.

-------, E -Y Hsie and Y.-H. Kuo, 1987: Description of the Penn State/NCAR mesoscale model version 4 (MM4) NCAR Tech Note, NCAR / TN-282, 66 pp.

Aubert, E F., 1957: On the release of latent heat as a factor in large-scale atmospheric motions. *J. Meteor* , **14**, 527-542

Augustine J A., and E J Zipser, 1987: The use of wind profilers in a mesoscale experiment. *Bull. Amer. Meteor Soc* , **68**, 4-17.

Akakawa, A., and V.R Lamb, 1977: Computational design of the basic dynamical process of the UCLA general circulation model *Methods in Computational Physics*, **17**, Academic Press, 173-265.

Bartels D.L , and R A Maddox, 1991: Midlevel cyclonic vortices generated by mesoscale convective systems. *Mon. Wea. Rev.*, **119**, 104-118.

Bélair, S , D.-L. Zhang and J. Maillot, 1993: Numerical prediction of the 10-11 June 1985 squall line with the Canadian regional finite-element model Submitted to *Weather and Forecasting.*

Biggerstaff, M.I , and R.A. Houze, Jr., 1991a: Kinematic and precipitation structure of the 10-11 June 1985 squall line. *Mon. Wea. Rev.*, **119**, 3034-3065.

--------, and --------, 1991b. Mid-level vorticity structure of the 10-11 June 1985 squall line. *Mon. Wea. Rev* , **119**, 3066-3079.

Blackadar, A K , 1979: High resolution models of the planetary boundary layer *Advances in Environmental Science and Engineering*, **1**, No. 1, Pfafflin and Ziegler, eds., Gordon and Breach Sci. Pub , New York, 50-85.

Bosart, L. F., 1981. The Presidents' Day snowstorm of 18-19 February 1979: A sub-synoptic-scale event. *Mon. Wea. Rev.*, **109**, 1542-1566.

--------, and F Sanders, 1981. The Johnstown flood of July 1977: A long-lived convective storm. *J. Atmos. Sci.*, **38**, 1616-1642.

Brandes, E.A., 1990: Evolution and structure of the 6-7 May 1985 mesoscale convective complex and associated vortex. *Mon Wea. Rev.*, **118**, 109-127.

Brown, J., and K. Campana, 1978: An economical time-differencing system for numerical weather prediction. *Mon. Wea. Rev.*, **106**, 1125-1136.

Carlson, T.N., and F.H. Ludlam, 1968: Conditions for the occurrence of severe local storms *Tellus*, **20**, 203-226.

Chang, C.B., D.J. Perkey and C.W. Kreitzberg, 1982: A numerical case study of the effects of latent heating on a developing wave cyclone. *J. Atmos Sci.*, **39**, 1555-1570

Charba J.P. and W.H. Klein, 1980: Skill in Precipitation forecasting in the national weather service *Bull. Amer. Met. Soc.*, **61**, 1546-1555.

Charney, J.G., 1947: The dynamics of long waves in a baroclinic westerly current. *J. Meteorol*, **4**, 135-163.

Charney, J.G., and A. Eliassen, 1964: On the growth of the hurricane depression. *J. Atmos Sci*, **21**, 68-75.

Cunning, J.B., 1986: The Oklahoma-Kansas Preliminary Regional Experiment for STORM-Central. *Bull. Amer. Meteorol. Soc.*, **67**, 1478-1486.

Danard, M.B., 1964: On the influence of released latent heat on cyclone development. *J. Appl. Meteor.*, **3**, 27-37.

-------- 1966: On the contribution of released latent heat to changes in available potential energy. *J. Appl. Meteor.*, **5**, 81-84.

Davis, C.A., and K. A. Emanuel, 1991: Potential vorticity diagnosis of cyclogenesis. *Mon. Wea. Rev.*, **119**, 1929-1953

--------, M.T. Stoelinga and Y.-H. Kuo, 1993: The integrated effect of condensation in numerical simulations of extratropical cyclogenesis. *Mon Wea Rev.*, **121**, 2309-2330

Dudhia, J., 1989: Numerical study of convection observed during the winter monsoon experiment using a mesoscale two-dimensional model. *J Atmos. Sci.*, **46**, 3077- 3107.

Eady, E. T., 1949: Long waves and cyclone waves. *Tellus*, **1**, 33-52.

Fritsch, J.M. and C.F. Chappell, 1980: Numerical prediction of convectively driven mesoscale pressure systems Part I: Convective parameterization *J Atmos. Sci*, **37**, 1722-1733.

--------, R.J. Kane and C R. Chelius, 1986: The contribution of mesoscale weather systems to the Warm-Season precipitation in the United States. *J. of Clim. and Appl. Meteor.*, **25**, 1333-1345.

--------, and K.F. Heideman, 1989: Some characteristics of the Limited- Area Fine-Mesh (LFM) Model quantitative precipitation forecasts (QPF) during the 1982 and 1983 Warm Seasons. *Weather and Forec.*, **2**, 173-185.

--------, J.D. Murphy and J.S. Kain, 1993: Mesoscale warm-core vortex amplification over land. Accepted by *J. Atmos. Sci.*.

Fujita, T.T., 1955: Results of detailed synoptic studies of squall lines. *Tellus*, **7**, 405-436.

Georgakakos K.P. and Hudlow, M.D., 1984: Quantitative precipitation forecast techniques for use in hydrologic forecasting. *Bull. Amer. Meteor. Soc.*, **65**, 1186-1200.

Glahn H.R , 1985: Yes, Precipitation forecasts have improved. *Bull. Amer. Meteor. Soc.*, **66**, 820-830

Gyakum, J.R., 1983. On the evolution of the *QE II* storm. II: Dynamic and thermodynamic structure. *Mon. Wea. Rev.*, **111**, 1156-1173.

Heideman, F.K. and J.M. Fritsch, 1988: Forcing mechanisms and other characteristics of significant summertime precipitation *Weather and Forecasting*, **3**, 115-130.

Holton, J. R., 1979: An introduction to dynamic meteorology. *Academic Press*, 391 pp.

Hoskins, B.J., M.E. McIntyre and A.W. Robertson, 1985: On the use and significance of isentropic potential vorticity maps. *Quart. J. Roy. Meteor. Soc.* **111**, 877-946.

Houze, R.A., Jr., 1977: Structure and dynamics of a tropical squall line system. *Mon. Wea. Rev.*, **105**, 1540-1567.

--------, B.F. Smull and P. Dodge, 1990: Mesoscale organization of springtime rainstorms in Oklahoma. *Mon. Wea. Rev.*, **118**, 613-654.

--------, S.A. Rutledge, M.I Biggerstaff, and B.F. Smull, 1989: Interpretation of Doppler weather radar displays of midlatitude mesoscale convective systems. *Bull. Amer. Meteor Soc.*, **70**, 608-617.

Hoxit, L R., C.F. Chappell and J.M. Fritsch, 1976: Formation of mesolows or pressure troughs in advance of cumulonimbus clouds. *Mon. Wea. Rev.*, **104**, 1419-1428.

Hsie, E-Y., R.A. Anthes, and D. Keyser, 1984: Numerical simulation of frontogenesis in a moist atmosphere. *J. Atmos. Sci.*, **41**, 2581-2594.

Johnson R.H , and D.L Bartels, 1992: Circulations associated with a mature-to-decaying midlatitude mesoscale convective system. Part II: Upper-level features. *Mon Wea Rev.*, **120**, 1301-1320

-------, and P J. Hamilton, 1988: The relationship of surface pressure features to the precipitation and airflow structure of an intense midlatitude squall line. *Mon. Wea. Rev.*, **116**, 1444-1471.

Kuo H.L., 1965: On formation and intensification of tropical cyclones through latent heat release by cumulus convection. *J. Atmos. Sci.*, **22**, 40-63.

Kuo, Y.-H., M.A. Shapiro, and E.G. Donall, 1991: The interaction between baroclinic and diabatic processes in a numerical simulation of a rapidly intensifying extratropical marine cyclone *Mon. Wea. Rev.*, **119**, 368-384.

Kutzbach, G., 1979: The thermal theory of cyclones *American Meteorological Society*, 255 pp.

Leary, C.A., and E.N. Rappaport, 1987: The life cycle and internal structure of a mesoscale convective complex. *Mon. Wea. Rev.*, **115**, 1503-1527.

Margules, M., 1903: Über die Energie der Stürme. *Jahr. kaisk. Zent. für Meteor , Vienna* (English translation by C. Abbel, 1910, *Smithsonian Misc. Coll.*, Washington, D C., **51**, 533-595).

Menard, R.D., and J.M. Fritsch, 1989: A mesoscale convective complex-generated inertially stable warm core vortex. *Mon. Wea. Rev.*,**117**, 1237-1261.

Murphy, J.D., and J.M. Fritsch, 1989: Multiple production of mesoscale convective systems by a convectively-generated mesoscale vortex. *12th Conference on weather analysis and forecasting*.

Newton, C.W., 1950: Structure and mechanism of the prefrontal squall line *J Meteor.*, **7**, 210-222.

Ogura, Y. and M.T. Liou, 1980: The structure of a Midlatitude squall line. A case study. *J. Atmos. Sci.*, **37**, 553-567.

Pauley, P.M., and P.J. Smith, 1988: Direct and indirect effects of latent heat release on a synoptic-scale wave system. *Mon. Wea. Rev.*, **116**, 1209-1235.

Perkey, D.J., and C.W. Kreitzberg, 1976: A time-dependent lateral boundary scheme for limited-area primitive equation models. *Mon. Wea. Rev.*, **104**, 744-755.

Ramage C.S., 1982: Have precipitation forecasts improved? *Bull. Amer. Meteor. Soc.*, **63**, 739-742.

Riehl, H. and J.S. Malkus, 1961: Some aspects of hurricane Daisy, 1958 *Tellus*, **13**, 181-213.

Rutledge, S. A., R.A. Houze, Jr., M.I Biggerstaff and T. Matejka, 1983: The Oklahoma-Kansas mesoscale convective system of 10-11 June 1985: Precipitation structure and single-Doppler radar analysis. *Mon. Wea. Rev.*, **116**, 1409-1430.

Sanders F, 1986: Trends in skill of Boston forecasts made at MIT, 1966-1984 *Bull. Amer. Meteor. Soc.*, **67**, 170-176.

Smith, P.J., P.M. Dare, and S.-J. Lin: 1984: The impact of latent heat release on synoptic-scale vertical motions and the development of an extratropical cyclone system. *Mon.Wea. Rev.*, **112**, 2421-2430.

Smull, B F., and R A. Houze, Jr , 1985· A midlatitude squall line with a trailing region of stratiform rain. Radar and satellite observations. *Mon. Wea. Rev.*, **113**, 117-133.

--------, and --------, 1987. Rear-inflow in squall lines with trailing stratiform precipitation. *Mon. Wea. Rev.*, **115**, 2869-2889.

Staley, D O., and R.L. Gall, 1977: On the wavelength of maximum baroclinic instability. *J. of Atmos Sci* , **34**, 1679-1688

Tracton, M.S., 1973. The role of cumulus convection in the development of extratropical cyclones. *Mon. Wea. Rev.*, **101**, 573-593.

Uccellini, L.W., R.A. Pettersen, K F. Brill, P.J. Kocin, and J.J. Tuccillo, 1987: Synergistic interactions between an upper-level jet steak and diabatic processes that influence the development of a low-level jet and a secondary coastal cyclone. *Mon. Wea. Rev.*, **115**, 2227-2261

Wetzel, P.J., W.R. Cotton and R.L. McAnally, 1983: A long-lived mesoscale convective complex. Part II. Evolution and structure of the mature complex. *Mon. Wea. Rev.*, **111**, 1919-1937.

Zhang, D.-L., 1992: The formation of cooling-induced mesovortex in the trailing stratiform region of a midlatitude squall line. *Mon. Wea Rev.*, **120**, 2763-2785.

--------, and Cho, 1992. The development of negative moist potential vorticity in the stratiform region of a simulated squall line. *Mon. Wea. Rev.*, **120**, 1321-1341.

--------, and J. M. Fritsch, 1988a· Numerical sensitivity experiments of varying model physics on the structure, evolution and dynamics of two mesoscale convective systems. *J. Atmos. Sci.*,**45**, 261-293.

--------, and --------, 1988b: A numerical investigation of a convectively generated, inertially stable, extratropical warm-core mesovortex over land. Part I· Structure and evolution. *Mon. Wea. Rev.*, **116**, 2660-2687.

--------, and --------, 1986: Numerical Simulation of the Meso–β Scale Structure and Evolution of the 1977 Johnstown Flood. Part I: Model Description and Verification. *J.Atmos. Sci.*, **43**, 1913-1943.

--------, and --------, 1987: Numerical simulation of the meso–β scale structure and evolution of the 1977 Johnstown flood. Part II: Inertially stable warm-core vortex and the mesoscale convective complex. *J. Atmos. Sci.*, **44**, 2593-2612.

--------, 1989: The effect of parameterized ice microphysics on the simulation of vortex circulation with a mesoscale hydrostatic model. *Tellus*, **41A**, 132-147.

--------, E.-Y. Hsie and M.W. Moncrieff, 1988: A comparison of explicit and implicit predictions of convective and stratiform precipitating weather systems with a meso-β-scale numerical model. *Q. J. Roy. Meteor. Soc.*, **114**, 31-60.

--------, K. Gao and D.B. Parsons, 1989: Numerical simulation of an intense squall line during 10-11 June 1985 PRE-STORM. Part I: Model verification. *Mon. Wea. Rev.*, **117**, 960-994.

--------, and K. Gao, 1989: Numerical simulation of an intense squall line during 10-11 June 1985 PRE-STORM. Part II: Rear inflow, Surface pressure perturbations and stratiform precipitation. *Mon. Wea. Rev.*, **117**, 2067-2094.

--------, H.-R. Chang, N.L. Seaman, T.T. Warner and J.M. Fritsch, 1986: A two-way interactive nesting procedure with variable terrain resolution. *Mon. Wea. Rev.*, **114**, 1330-1339

--------, and R.A. Anthes, 1982: A high-resolution model of the planetary boundary layer—sensitivity tests and comparison with SESAME-79 data. *J. Appl. Meteor.*, **21**, 1594-1609.